Energy & Environmental Science

REVIEW

View Article Online
View Journal

Cite this: DOI: 10.1039/c5ee03698d

Mass transport aspects of electrochemical solar-hydrogen generation

Miguel A. Modestino,* S. Mohammad H. Hashemi and Sophia Haussener

The conception of practical solar-hydrogen generators requires the implementation of engineering design principles that allow photo-electrochemical material systems to operate efficiently, continuously and stably over their lifetime. At the heart of these engineering aspects lie the mass transport of reactants, intermediates and products throughout the device. This review comprehensively covers these aspects and ties together all of the processes required for the efficient production of pure streams of solar-hydrogen. In order to do so, the article describes the fundamental physical processes that occur at different locations of a generalized device topology and presents the state-of-the-art advances in materials and engineering approaches to mitigate mass-transport challenges. Processes that take place in the light absorber and electrocatalyst components are only briefly described, while the main focus is given to mass transport processes in the boundary-layer and bulk liquid or solid electrolytes. Lastly, a perspective on how engineering approaches can enable more efficient solar-fuel generators is presented.

Received 8th December 2015,
Accepted 1st March 2016

DOI: 10.1039/c5ee03698d

www.rsc.org/ees

Broader context

Solar-hydrogen generators have the potential to trigger the incorporation of a much larger share of solar energy sources in our current energy landscape. These technologies can directly capture and store energy from the sun in the form of hydrogen molecules. As hydrogen can be transported, and stored for long periods of time, solar-hydrogen devices allow for the spacio-temporal decoupling of the energy generation and consumption processes, and in this way provide a larger flexibility to the electrical grid. While significant focus has been given to the development of photoelectrochemical materials for solar water-splitting, equally important are engineering aspects related to the materials' integration into devices that can operate stably, and produce pure hydrogen streams continuously over long lifetimes. This review provides a broad view on these engineering challenges and approaches to conceive practical solar-hydrogen generators.

School of Engineering, École Polytechnique Fédéral de Lausanne (EPFL), Station 17, 1015, Lausanne, Switzerland. E-mail: miguel.modestino@epfl.ch; Tel: +41 21 69 33446

Miguel A. Modestino

Dr Miguel Modestino is a post-doctoral researcher and project manager of the Nanotera-SHINE project at the Ecole Polytechnique Fédérale de Lausanne (EPFL). He obtained his BS in Chemical Engineering (2007), MS in Chemical Engineering Practice (2008) from the Massachusetts Institute of Technology, and his PhD in Chemical Engineering from the University of California, Berkeley (2013). His PhD work involved transport and self-assembly aspects of solar-fuels membranes, and currently his research focuses on electrochemical engineering and materials aspects of solar-hydrogen generators. His research interests lie at the interface of electrochemical energy conversion devices and functional polymer composites.

S. Mohammad H. Hashemi

S. Mohammad H. Hashemi received his BSc and MSc in mechanical engineering with a focus on Thermo-fluid Sciences from University of Tehran, Iran. Since 2012 he has been working towards a PhD degree in Microtechnology at École Polytechnique Fédéral de Lausanne (EPFL), Switzerland. He has designed and fabricated micro-reactors for renewable energy applications such as chemical fuel production and water decontamination. His multidisciplinary research lies at the interface of microfabrication, electrochemistry, fluid mechanics, and heat transfer.

1. Introduction

The ability to reliably supply the world with clean, and renewable energy relies strongly on the development of energy storage solutions that can dampen the inherent intermittency of electricity production from sources such as wind and solar.[1–3] Undeniably, pumped hydroelectrical power accounts for the vast majority of the current energy storage capacity – 140 GW or 99.3% of the overall global storage capacity in 2013 – but it only represents 6% of electricity production.[4] Despite its predominance, the ability to store energy hydroelectrically is directly bound to regional topographical constrains and usually leads to severe ecological disruption as large portions of land are artificially flooded. More attractive solutions that have been at the centre of discussion include the large scale implementation of batteries or hydrogen (H_2) production. The former alternative represents a simple solution for stationary applications or for use in small vehicles with limited range; as recently demonstrated by notable examples of battery powered vehicles and distributed residential energy storage. On the other hand, hydrogen is a fuel that has the advantage to be transportable, easy to implement in mobile applications, and the ability to reach large scale storage capacity. Moreover, hydrogen has the potential to store renewable energy across seasons and locations – such that solar energy may be harvested and transformed into fuels at locations of high irradiation during the summer and then redistributed to low-irradiation regions or used when solar resources are scarce in the winter. Stand-alone photo-electrochemical solar-hydrogen generators are an attractive technology, as their implementation wouldn't disrupt the current electricity grid and potentially relax its constraints. This review will focus on photo-electrochemical solar-hydrogen generators, which represent one of the most promising technologies to disruptively increase the share of renewables in our global energy portfolio. Specifically, the discussion presented here will be centred on the progress in chemical engineering approaches to solar-hydrogen production and, in particular, of their mass transport aspects.

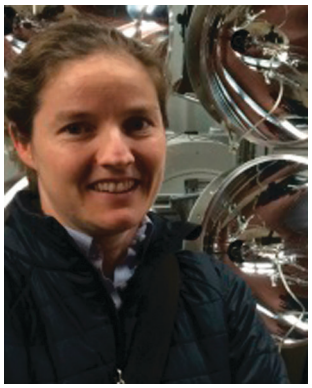

Sophia Haussener

Sophia Haussener is an Assistant Professor heading the Laboratory of Renewable Energy Science and Engineering at the Ecole Polytechnique Fédérale de Lausanne (EPFL). Her current research is focused on providing design guidelines for thermal, thermo-chemical, and photoelectrochemical energy conversion reactors through multi-physics and multi-scale modeling and experimentation. Her research interests include: thermal sciences, fluid dynamics, charge transfer, electro-magnetism, and thermo/electro/photochemistry in complex multi-phase media on multiple scales. She received her MSc (2007) and PhD (2010) in Mechanical Engineering from ETH Zurich. She was a postdoctoral researcher at the Joint Center of Artificial Photosynthesis (JCAP) and the Lawrence Berkeley National Laboratory (LBNL) between 2011 and 2012.

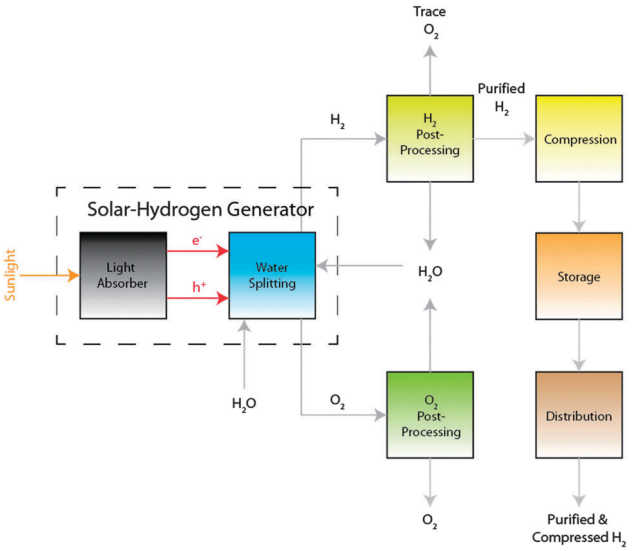

Fig. 1 Flow diagram of the processes involved in the production of on-demand, compressed solar hydrogen. The heart of the operation is carried by the solar-hydrogen generator. This units takes as inputs sunlight and water to produce H_2 gas, which then undergoes a series of downstream processes to obtain purified and compressed H_2 ready for utilization.

While the focus of this review is on the processes involved within a solar-H_2 generator, the overall operation required to produce solar hydrogen involves the implementation of these devices together with a set of downstream steps that result in purified and compressed H_2. Fig. 1 presents an example flow diagram for a prototypical solar H_2 production plant. There, H_2 and oxygen (O_2) are generated from sunlight and water, and then processed so that water is extracted from the gas streams and recirculated into the water-splitting units. O_2 can either be released into the environment or collected as a byproduct and valorized for alternative applications. The H_2 fuel stream undergoes further compression, storage and distribution processes in order to reach consumers at the required levels of purity and pressure. Purposely, this review article will not focus on the progress in photoelectrochemical water-splitting materials, but rather refer readers to comprehensive reviews that have been recently published on the topic.[5–13] Instead, here we will review engineering approaches to manage the interacting physical transport processes involved in photo-electrochemical solar-hydrogen production as well as present a balanced discussion around the challenges and considerations that need to be overcome for solar-hydrogen technologies to be deployed.

2. Definition of components and processes in solar-hydrogen generation

Solar-hydrogen generator devices are the core of the solar-hydrogen production process. These devices need to simultaneously capture

sunlight, generate charge carriers, and transport them to catalytic sites where the oxygen and hydrogen evolution reaction takes place. Ions need to be transported between reaction sites and the evolved hydrogen and oxygen needs to be collected in separate streams, with compositions below the flammability limit. For consistency, these processes will be referred as:

(1) Light absorption (LA): encompassing the absorption of sunlight in a semiconductor and the generation of charge carrier pairs.

(2) Electronic charge transport (ECT): involving the transport of charge carriers (*i.e.* electrons and holes) from the generation location to the catalytic centres or semiconductor/liquid interface.

(3) Electrochemical reactions (ER): including both the hydrogen and oxygen evolution process.

(4) Transport of neutral species (TNS): accounting for the transport of water and products in liquid or gas phase.

(5) Transport of charged species (TCS): which includes the transport of ionic species between reaction sites.

Each of these processes will take place at different locations within the device as depicted in Fig. 2. The light absorption and electronic charge transport processes take place volumetrically within the semiconductor. The electrochemical reactions happen at the interface between either a semiconductor or a catalyst and the electrolyte. In the electrolyte region close to this interface, transport processes of reactants, ions and products will take place within a mass transport boundary layer. Mass transport of all species will also occur within the bulk electrolyte which can be either a liquid electrolyte or a solid-state ion-conducting membrane.

Lastly, all of the processes defined above will be modified depending on the operating conditions of the device. For simplicity purposes this review will cover three main categories of operation for these systems: operated under liquid electrolytes, under liquid water (de-ionized), and under water vapor. When the device is operated under liquid electrolytes the electrochemical reactions will take place at the semiconductor or catalyst/liquid interface. For devices operated with liquid and vapor water, the reactions will take place at the interface between the inorganic components and the ion-conducting membrane. The main difference between these last two scenarios, is that the low concentration of water in the vapor phase poses significant challenges for devices operated at high production rates, as the transport of water can become limiting.

3. Internal processes in solar-hydrogen devices

The previous section of this review defined the processes, device components and locations that compose a solar-hydrogen generator. Through this section of the review we will describe the operation of the device at each of the locations defined above. While doing so, approaches to mitigate challenges and limitations are presented and the interactions between each component of devices are highlighted.

3.1 Processes in the semiconductor

The semiconductor is responsible for absorbing light, and generating the charge carriers necessary to carry out the electrochemical reactions (Fig. 3). As multiple comprehensive reviews on semiconductor materials for solar water-splitting have been recently published in the literature,[6,14–19] we will limit this section to a summary of the processes taking place within this component.[16,20]

The propagation of the irradiated light toward and within the semiconductor is described by Maxwell's equations. The absorbed energy and the optical quantum yield define the rate of the charge carrier pair density generation. This process can be simplified to the Beer–Lambert law for homogeneous semiconductor films.[21–23] Following this simplification, the change in light intensity is described by an exponential decrease with penetration depth, and the extinction coefficient of the material defines the extent of this decay. Usually, the Beer–Lambert law

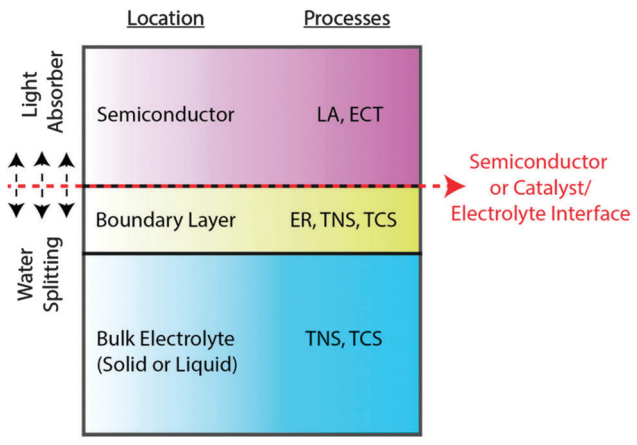

Fig. 2 Device topology identifying the location of different processes required for solar water-splitting. These processes include light absorption (LA), electronic charge transport (ECT), electrochemical reactions (ER), transport of neutral species (TNS), and charged species (TCS).

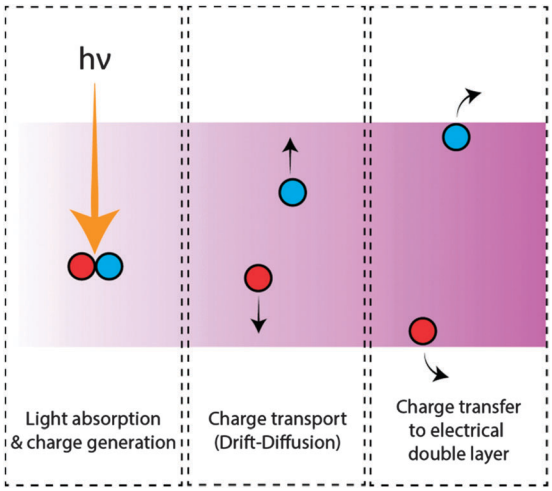

Fig. 3 Diagram of processes involved in the semiconductor. The scheme depicts the absorption, charge generation, transport and transfer process required to drive the electrochemical reactions of solar-hydrogen generators.

allows for a simple approximation of the charge generation term, but is unable to accurately quantify the absorbed radiation in non-planar, heterogeneous, and anisotropic absorbers.[24,25] The radiation absorption analysis has to be adapted to account for scattering effects of bubbles and absorption in the electrolyte if the photoabsorber is covered by electrolyte.[26]

Once charge carriers are generated, they need to be transported to the interface of the semiconductor so as to participate in the electrochemical reactions. The transport of these charge carriers is usually driven by carrier concentration gradients (diffusion) and electric fields (drift). This diffusion-drift model can be described as,

$$\boldsymbol{j}_i = -D_i \nabla c_i + z_i c_i \mu_i \boldsymbol{E} \quad (1)$$

where $\boldsymbol{j}_i$ is the net carriers flux of the charge carrier i, D_i its diffusion coefficient, c_i its local concentration, z_i its charge, μ_i its mobility and $\boldsymbol{E}$ the electric field affecting it. In the case of systems exhibiting a direct semiconductor–electrolyte interface, an electric field – the so called space charge layer – will evolve near this interfacial region and will drive charge separation. In the bulk of the semiconductor, concentration gradients will dominate the charge transport behavior. Overall, the carrier concentration distribution can be defined by the charge conservation equation,

$$\frac{\partial c_i}{\partial t} = \nabla \cdot \boldsymbol{j}_i + G - R_i \quad (2)$$

so that the charge accumulation over time (t), depends on the balance between generation rate (G), recombination rate (R_i) and the flux of carriers. Recombination is typically dominated by Shockley–Reed–Hall, radiative, Auger, and surface recombination.

The charge transport process described above will define the overall flux of charges towards the electrochemical reaction sites, and the rate at which hydrogen is evolved in the solar-hydrogen generator device.

3.2 Processes in the boundary layer

The boundary layer is defined as the region of the electrochemical cell in close proximity to the catalytic surfaces where important concentration or velocity gradients can evolve. The boundary layer is bounded by the hydrogen or oxygen evolutions reactions sites (HER and OER respectively) and the bulk electrolyte. Within this subsection we will briefly describe the factors that define the electrocatalytic rates observed at the surface of the electrodes, the formation and structure of the electrical double layer at the interface between the semiconductor or catalyst (metal or insulator) and the electrolyte, and how the reaction kinetics will affect the characteristics of the boundary layers of systems operated under liquid or solid-state electrolytes. Fig. 4 shows a diagram of all the processes involved in this region.

Electrode reactions. For solar-hydrogen devices the half-reactions that take place on the surface of the semiconductor or the heterogeneous electrocatalyst can be written as:

$$H_2O \rightarrow 2H^+ + 1/2O_2 + 2e^- \text{ (anode)}$$

$$2H^+ + 2e^- \rightarrow H_2 \text{ (cathode)}$$

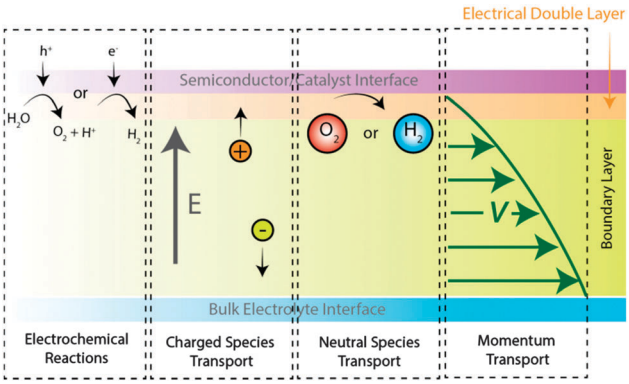

Fig. 4 Diagram of processes involved in the boundary layer. Electrochemical reactions take place at the interface with the catalyst or semiconductor, neutral and charged species migrate and diffuse across the boundary layer, and a velocity gradient evolves from the interface.

in acidic electrolytes, or

$$2OH^- \rightarrow 1/2O_2 + H_2O + 2e^- \text{ (anode)}$$

$$2H_2O + 2e^- \rightarrow H_2 + 2OH^- \text{ (cathode)}$$

under basic conditions. For metal–electrolyte and approximatively also semiconductor–electrolyte interfaces, a generalized Buttler–Volmer expression can closely describe the rate of each of these reactions,

$$\boldsymbol{j} = j_0 \left[\left(\frac{c_{\text{red,surf}}}{c_{\text{red,bulk}}} \right)^{\gamma_1} \exp\left(\frac{\alpha_a F \eta}{RT} \right) - \left(\frac{c_{\text{ox,surf}}}{c_{\text{ox,bulk}}} \right)^{\gamma_2} \exp\left(-\frac{\alpha_c F \eta}{RT} \right) \right] \hat{\boldsymbol{n}} \quad (3)$$

where $\boldsymbol{j}$ is the current density (positive for anodic currents) in the direction, $\hat{\boldsymbol{n}}$, normal to the electrode surface. j_0 is the exchange current density, α_a and α_c are the apparent transfer coefficients for the anodic and cathodic reactions, and η is the electrode surface overpotential.[27] c_{surf} and c_{bulk} correspond to the surface and bulk concentration of species involved in the cathodic reaction (red) or the anodic reaction (ox). The contribution of these concentration terms are determined by the exponents γ_1 and γ_2.

The parameters that define the current levels (j_0 and α) are strongly dependent on material properties, surface treatments, and solution composition. Commercial water splitting systems that operate under acidic environments often implement electrocatalysts based on platinum (Pt) and iridium oxide (IrO_x) for the HER and OER respectively, while their alkaline counterparts use Nickel based catalysts. Significant research efforts have been devoted to develop novel catalysts with the aim of improving the efficiency of the state-of-the-art materials, or to identify earth-abundant substitutes to the Pt or IrO_x-based catalysts. Multiple reports in the literature have covered the developments of this field,[6,28–32] and some efforts have been devoted to benchmark the performance of materials under comparable operating conditions.[33,34] These efforts are of great value to the development of solar-hydrogen generators, as the unifying

metrics measured for various electrocatalyst systems can directly aid in the design of practical devices.

The electrical double layer. The electrical double layer describes two charged regions in close vicinity of the electrode surface, usually in a dimensional-scale of several nanometers (Fig. 5). Assuming ideally polarizable electrodes, the layers evolve as a result of specific adsorption of solvent molecules or ions species on the electrode with resulting bond formation, and electrostatic attraction due to an applied potential in the electrode. These two effects result in a polarized layer close to the surface with a thickness in the range of Angstroms (typical radius of adsorbed ions). This layer is composed of the adsorbed molecules and ions (also called inner Helmholtz layer), and solvated ions with the counter-charge of the surface (building the outer Helmholtz layer). Next to the Helmholtz layer there is a layer composed of solvated anions and cations, with the net electrical charge equal to the sum of the surface charge of the electrode and the charge of the Helmholtz layer. This outer layer, also called diffuse layer, is loosely attracted to the charge interface as a result of long-range forces (electrostatic forces) and exhibits an extended dimension. The thickness of the diffuse layer is a function of the electrolyte properties only, namely its bulk concentration, its relative permittivity, ion charges, and temperature. The Debey length can be used to estimate the thickness of the diffuse layer, which is usually in a range of several nm. This is in contrast to the liquid electrolyte boundary layer resulting from the no-slip boundary condition and the corresponding fluid flow distribution (discussed in the next section), which is electrically neutral and spans a significantly larger area, usually in the range of micrometers to millimeters.

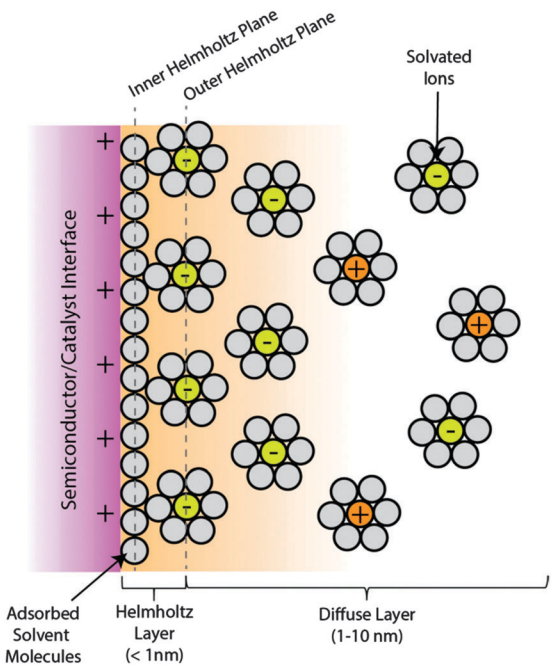

Fig. 5 Schematic representation of the electrical double layer. The positive (+) and negative (−) species represent solvated ions which compose the Helmholtz layer as well as the diffuse layer.

Historically, the electrical double layer has been described by Helmholtz, reformulated by Gouy–Chapman, combined by Stern, and further detailed by Graham.[35,36] The Helmholtz and the diffuse layers can be represented as two capacitors in series. For large electrolyte concentrations, the total capacitance is dominated by the capacitance in the Helmholtz layer and so is the potential drop over the double layer. These conditions can be used in experimental investigations in order to simplify the interpretation of the data.

In contrast to metal electrodes, the carrier density in semiconductor is much smaller, resulting in a distribution of the surface charge over a finite depth, *i.e.* the space charge layer. The electrical double layer is affected by this space charge layer and eventually the potential drop over the interface is influenced by the three layers in series: the space charge layer in the semiconductor, the Helmholtz layer, and the diffuse layer. The potential drop distribution across the three layers is dependent on the materials and operating conditions.

The double layer affects phenomena such as charge transport in small scale structures (nano- to micron-scale),[37] and electrophoretic or electroosmotic effects.[38] The electrical double layer can also be used to probe the nanorheology of the solvent and ion system at the charged surface.[39] In (photo)electrochemical applications, the double layer affects the amount of current used in the electrochemical reaction as it acts as a capacitor in parallel with the surface reaction:[27]

$$\boldsymbol{j}\cdot\hat{\boldsymbol{n}} = f(\eta, c_i) + C\frac{\mathrm{d}\eta}{\mathrm{d}t} \qquad (4)$$

where f is the function describing the electrode kinetics, C is the capacity of the double layer, and c_i the species concentration in the bulk. The actual current used for the charging and discharging of the double layer depends heavily on the applied potential, the frequency or alternation of the current (*e.g.* resulting from transient irradiation), the interface characteristics (electrode material, surface roughness), and the electrolyte composition. Additionally, the microscopic architecture of the double layer affects the details of the charge transfer to the surface and the elementary steps of the electrode kinetics. A semi-empirical correction to eqn (4) consist of adapting the concentration from the bulk concentration to the concentration at the interface between the Helmholtz and diffuse layer, and reducing the overpotential by the potential drop in the Helmholtz layer.[27]

Novel insights on the structure of and charge transport within the double layer and its effect on charge transport to and from the surfaces and its influence on the surface kinetics have been provided by the utilization of detailed molecular dynamics simulations.[40]

Liquid electrolyte boundary layers. While the electrical double layer describes the first few nanometers of the interface between the electrolyte and the reaction sites, there is a much larger region in close proximity with this interface where the properties of the electrolyte (*i.e.* momentum and composition) are not uniform – the mass transport boundary layer. Its thickness (δ_c) can be best estimated using dimensionless numbers such as

the Sherwood number, Sh = $k\delta_c/D$, which relates the mass transfer coefficient (k) for species' transport from the bulk to the surface or *vice versa* with their diffusion coefficient (D). The Sherwood number is usually given as a function of Reynolds number, Re = $xu_0\rho/\mu$, and Schmidt number, Sc = $\mu/(\rho D)$, where x is a characteristic system dimension, u_0 the average linear velocity of the fluid, ρ its density and μ its kinematic viscosity. The actual functional dependence will vary according to the flow field and the configuration. For the simple case of a laminar flow parallel to a flat plate, the estimation of the mass transport coefficient and the typical boundary layer thickness along the plane direction x is given by,[41]

$$\frac{\delta_c}{x} = 4.64 \cdot \mathrm{Re}^{-1/2}\mathrm{Sc}^{-1/3} \quad (5)$$

For different flow geometries similar expressions can be derived, but the exponents modifying the Re and Sc numbers will vary, as well as the proportionality constant.[42]

In electrochemical water splitting devices, the boundary layer will determine the extent of the mass transport limitations and ultimately the device performance. These limitations are best mitigated when devices are operated under strong acidic or basic electrolytes. Under these conditions, the transport of intermediate species (H^+ or OH^-) is not limiting, the electrode reactions occur at a higher rate, and the formation of ionic concentration gradients are minimized. Despite these advantages, only a few electrocatalytic or photoelectrocatalytic materials are stable under these highly corrosive electrolytes. Operating water splitting devices at moderate pH conditions in buffered electrolytes or supporting electrolytes can enhance the materials' stability to a limited extent. When buffered liquid electrolytes are used, the transport of charged species becomes complex. During operation, H^+ ions are produced in the surface of the anode while they are consumed at the cathode. This leads to the formation of a depletion zone at the vicinity of the cathode and an accumulation one in the anode. As the concentration of H^+ or OH^- ions is low in the buffered electrolyte, a pH gradient will evolve from the surface of the electrodes and a large portion of the current in the system will be carried by supporting ions. This in turn will result in the formation of further concentration gradients of supporting ions at the surface of electrodes, building up adverse potentials in the cell. These phenomena can significantly affect the cell current density at a given potential by imposing concentration polarization (CP) losses.[43] The extent of these losses can be assessed by balancing all the ionic transport processes occurring in the electrochemical cell (*i.e.* migration, diffusion and convection):

$$\boldsymbol{j} = -F^2\nabla\phi\sum_i z_i^2 u_i c_i - F\sum_i z_i D_i \nabla c_i + F\boldsymbol{u}\sum_i z_i c_i \quad (6)$$

where F, z_i, u_i, c_i, D_i, and, $\boldsymbol{u}$ are the Faraday's constant, species charge, mobility, concentration, diffusivity and electrolyte's velocity profile, respectively. The last (convection) term in the expression can be set to zero due to the electroneutrality condition. This expression is valid for dilute electrolytes, and it can take more complex forms in concentrated solutions. It is often convenient to define the conductivity of the electrolyte, κ, as,

$$\kappa = F^2\sum_i z_i^2 u_i c_i \quad (7)$$

and the potential losses in the systems as,

$$\nabla\phi = -\frac{\boldsymbol{j}}{\kappa} - \frac{F}{\kappa}\sum_i z_i D_i \nabla c_i \quad (8)$$

where the second term, the diffusion potential, directly describe the CP losses in the cell. As significant concentration gradients form at the surface of the electrodes, larger potentials will be required to achieve a given current density. It is also important to clarify that κ is not necessarily uniform through the electrochemical cell, and that the gradients formed will lead to variations in conductivity across the electrolyte. At the limit, if ions are depleted in a particular region of the cell, the conductivity will tend to zero. Thus, for the device to operate at practical current densities (*i.e.* >10 mA cm^{-2}), the concentration difference across the boundary layer should remain small. Analytical expressions for concentration profiles and resultant losses have been provided in a theoretical study.[44] Another consequence of the large difference between the H^+ or OH^- concentration at the surface of electrodes and the bulk electrolyte is the appearance of a highly corrosive medium in contact with the surface of the electrode materials. This is specifically important since in many cases buffered electrolytes are used to provide higher levels of flexibility over the catalyst selection.

Due to the problems referred above, several groups have started to implement techniques to probe the ionic concentrations and subsequent losses at the surface of electrodes.[45] Scanning electrochemical microscopy (SECM)[46] is a well established and versatile method capable of providing three dimensional pH maps close to the electrodes with submicron resolution.[47,48] It can also help to elucidate transient and steady state hydrogen evolution rates.[49] Apart from SECM, non-intrusive confocal fluorescent microscopy methods with pH sensitive dyes can be used to probe the pH variations in three dimensions close to the catalyst.[50] Additionally, some efforts have focussed on mitigating the CP losses around the boundary layer by implementing device engineering solutions. Recently, some studies have proposed the use of fast flow rates (forced convection) of liquid electrolytes in microfluidic channels to minimize the adverse effects of ion concentrations.[51] By increasing the convective transport near the electrodes, the size of the boundary layer can be reduced and the transport of ionic species enhanced. Under these conditions, the concentration gradients near the electrodes can be significantly reduced. A recent study has also shown that bubble-induced mixing near the surface of the electrodes can reduce the transport losses to less than 25 mV at 10 mA cm^{-2}. In the contrary, a stagnant cell had limiting currents below 3 mA cm^{-2}.[43]

Although the convective mixing due to the growth and movement of bubbles can be beneficial for the minimization of concentration losses, the presence of bubbles can have detrimental effects for a solar-hydrogen device. The bubbles can increase the reaction kinetic losses if they are not released

rapidly from the catalyst surface. Moreover, in integrated PEC devices, they can affect the light absorption in the semiconductor by inducing undesirable scattering and reflections. Few methods have been employed to relax these adverse effects. In an early example,[52] the surfactant Triton X-100 was added to the electrolyte in order to reduce the size of bubbles and encourage faster detachments. In a fully integrated PEC device,[53] a louvered architecture has been implemented to address the bubble related challenges. The photoanode and photocathode are placed at tilt angles with respect to two horizontal axes, so that the evolved gases could move towards devised outlets after sufficient growth. Apart from these notable examples, most of the demonstrated solar-hydrogen devices place electrodes vertically in an electrolyte and do not investigate the limitations that bubble transport imposes on these systems.[54–64] In these cases, the devices rely on the upward movement of bubbles due to buoyant forces towards collection sites. In a deployable integrated solar-fuel generator, this configuration will pose significant challenges, as the photoabsorber will need to be placed normal to solar irradiation direction. Moving forward, electrochemical system designs that can mitigate the transport challenges described above can have a strong impact in the development of solar-hydrogen devices.

Solid electrolyte boundary layers. When devices are operated with pure water or vapor, solid-state ion conductors are required to allow for ion-transport between the electrodes.[65,66] Under these circumstances the interfacial layer of the ionomer that covers the catalyst surface plays a very important role in defining the overall device performance. Mainly, this ionomer layer needs to allow for fast water, gas and ion transport between the surfaces of the catalyst into the bulk region of the device. These interfacial processes are critical in the catalyst layers of membrane electrode assemblies in water electrolyzers. In these systems, pure water is fed into the surface of catalysts layers, which are composed of blends of carbon particles (providing electrical conductivity), catalyst nanoparticles and ionomers such as Nafion (Fig. 6). Within the catalyst layers, water diffuses through the ionomer film onto the catalyst surface where the water oxidation or proton reduction reactions take place. Then protons migrate across thin ionomer films into the bulk membrane, while the evolved gases diffuse through the ionomer layer towards collection ports.[67,68] The overall morphology of the catalyst layer plays a key role, as mesoscale porosity is desired to alleviate mass transport limitations. Within state-of-the-art catalyst layers water and gases can readily flow across the porous structure, while they diffuse slowly through the ionomer films covering the catalyst particles. These ionomer films usually have thicknesses in the order of 10 nm which facilitates fast transport of species. In an effort to further improve the current throughput in catalyst layers, some research groups have started to developed high-surface area catalyst layers by templating electrocatalysts into microwire arrays.[69,70] These rationally designed structures have led to catalyst layers that can operate stably at current densities of several A cm^{-2}.

It is also worth noting that although Nafion is commonly used as the ionomer material in catalyst layers; its transport properties are not well suited for this task. Nafion exhibits high levels of ion-conduction but also is fairly impermeable to gases and water thanks to its semi-crystalline matrix (see Section 3.4 for additional details). These transport issues are aggravated in Nafion thin-films as confinement and wetting interaction effects can further limit the transport properties of this material.[71–77] Improving the gas and water permeation levels of the ionomer at this interface can enable devices that operate at higher current densities and improved water splitting efficiencies. This can be achieved by implementing hygroscopic polymeric binder materials with high water permeability and increased gas permeability through the water swollen regions of the material. The concepts and knowledge accumulated by studying catalyst layers for water-splitting devices can also be useful in solar-hydrogen generators. Photoactive membrane electrode assemblies based on TiO_2 have been recently demonstrated,[78] but there is still ample opportunities to achieve high-efficiency light driven fuel production in catalyst layers.

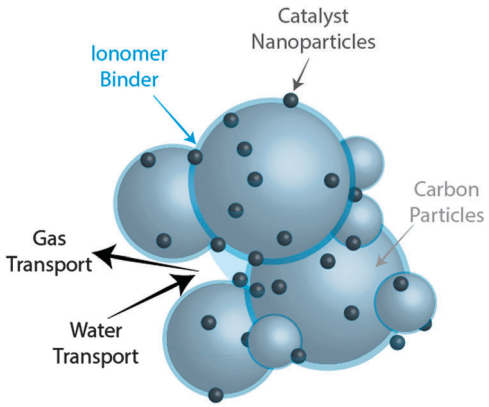

Fig. 6 Schematic representation of state-of-the-art catalyst layer describing the blend between conducting carbon particles, catalytic nanoparticles and ionomer binder. Water diffuses fast through the porous structure and into the ionomer thin-film towards the catalyst particles. The evolved gases will then diffuse through the ionomer films and transport out of the catalyst layer towards collection ports.

3.3 Processes in bulk liquid electrolytes

Within this review, the bulk liquid electrolyte is defined as the region of the device far from the electrode surface where the concentration of species can be considered to be approximately uniform. The bulk electrolyte is bounded by the boundary layers of the anode and/or cathode, and possibly a solid-electrolyte membrane. In a hydrogen generator, this region can be simple or compound. In a compound electrolyte, the ionic transport takes place in a combination of a separator and a supporting liquid electrolyte.[79,80] In general, the transport of species through the bulk electrolyte needs to satisfy two conditions: (i) deliver the product gases to independent collection ports with minimum levels of cross-contamination and (ii) provide a low-resistance pathway for ionic transport across the electrodes (Fig. 7). To satisfy the first conditions, devices are designed so that H_2 fuel is supersaturated in the electrolyte and collected in the gas phase at independent ports. Membranes are commonly proposed to

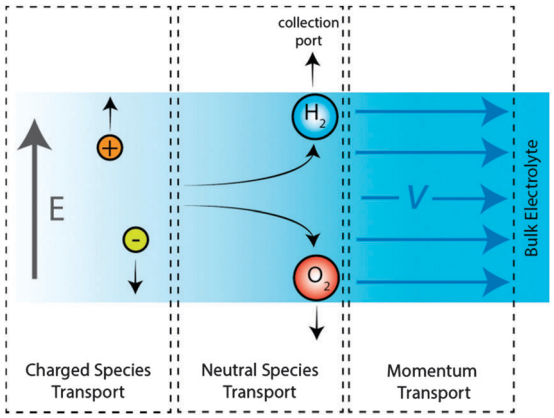

Fig. 7 Diagram of processes involved in the bulk electrolyte. Ions migrate between electrodes, products are transported towards collections sites by convection and diffusion, and convective flows can be used to mitigate transport limitations.

avoid undesirable levels of crossover. To reduce the ionic resistance of the system, the design of the device should minimize the interelectrode distance and incorporate electrolytes with high conductivities. Strong acid or base electrolytes have high conductivities and their use avoid the formation of large concentration gradients.

As mentioned in the previous section, some materials stability constraints can be mitigated to some extent by operating devices under moderate pH buffered electrolytes. As the concentration of OH^- and/or H^+ is low in buffered electrolytes, a significant fraction of the current in the system will be carried by supporting ions. When supporting electrolytes are used in membrane-separated systems, the bulk electrolyte in either side of the membrane can reach significantly different compositions, leading to CP losses as the ones observed in the electrode boundary layer. Several methods have been developed to address this challenge. Potentiometric measurements of buffered electrolytes in cells constructed with anion and cation exchange membranes suggest that the use of large volumes of electrolytes per unit electrode area can prevent depletion of the buffer capacity.[81] This method however, increases the size of the system which can hinder large scale deployment. Employing circulatory convective streams between the HER and OER compartments is another solution that can relax the concentration gradients problem without the need for utilization of large volumes of electrolytes.[82] The drawback is that by introducing recirculating streams, product crossover is also enhanced which affects the purity of the hydrogen fuel produced. This constrains the range of recirculating flowrates that can be implemented before the concentration of O_2 in the fuel stream reaches levels above the flammability limit. Another promising solution involves the employment of microfluidic approaches to reduce the volume of electrolyte, avoid the formation of large concentration gradients, and reduce the pathlengths for ion transport; overall reducing the cell overpotential. This is achieved by operating devices under electrolyte streams at high flow rates so that the boundary layer thickness is minimized. Although previous studies have shown effective, safe and robust production of oxygen-free hydrogen streams,[51,79] employing these principles in large-scale prototypes has yet to be demonstrated.

To better understand the transport processes that occur in the bulk electrolyte it is useful to describe the physical processes using the governing transport equations. Below, we describe these equations for conservation and transport of chemical species coupled to the Navier–Stokes equations through a convective term.[83]

The steady state mass conservation equation for charged or neutral species is given by,

$$-\nabla\cdot\boldsymbol{N}_i + r_i = 0 \tag{9}$$

Here $\boldsymbol{N}_i$ is the molar flux vector and r_i is a bulk reaction source term. Similar to eqn (6), the molar flux is given by,

$$\boldsymbol{N}_i = -z_i u_{i,e} F \nabla\phi_l - D_{i,e}\nabla c_i + \boldsymbol{u}c_i \tag{10}$$

where z_i, $u_{i,e}$, F, ϕ_l, $D_{i,e}$, c_i, and $\boldsymbol{u}$ are the species valence, effective mobility, Faraday's constant, potential of the liquid phase, species effective diffusivity, concentration, and liquid velocity, respectively. The effective diffusivity and mobility of charged species can be related by Nernst–Einstein equation: $u_{i,e} = D_{i,e}/(RT)$. The velocity profile can be obtained through the steady mass and momentum conservation (*i.e.* Navier–Stokes) equations for Newtonian and incompressible fluids,

$$\nabla\cdot\boldsymbol{u} = 0 \tag{11}$$

$$(\boldsymbol{u}\cdot\nabla)\boldsymbol{u} = -\frac{1}{\rho}\nabla p + \nu\nabla^2\boldsymbol{u} \tag{12}$$

where ρ, p, and ν are density, pressure, and kinematic viscosity, respectively. If a porous separator is used in the device, eqn (12) can be modified for the porous region following a Darcy's model for porous medium,

$$\left(\frac{\langle\boldsymbol{u}\rangle}{\varepsilon}\cdot\nabla\right)\frac{\langle\boldsymbol{u}\rangle}{\varepsilon} = -\frac{1}{\rho}\nabla p + \frac{\nu}{\varepsilon}\nabla^2\langle\boldsymbol{u}\rangle - \frac{\nu}{K}\langle\boldsymbol{u}\rangle \tag{13}$$

where ε and K are porosity and permeability of the fluid through the separator. In this case, $\langle\boldsymbol{u}\rangle$ is the superficial velocity vector: an equivalent velocity field that allows for the treatment of the flow as if it was confined to a one-phase media. The last term on the right side is added to account for viscous losses in the porous separator. In the case of a uniform liquid electrolyte, this equation reduces to eqn (12) as porosity tends to unity, permeability to infinity, and superficial velocity is replaced by the actual fluid velocity, $\boldsymbol{u}$. In all equations presented above, isotropic properties such as diffusivity, porosity, and permeability are assumed. By solving this set of equations, all important operational parameters can be estimated: overpotentials, product crossover, concentration, and velocity profiles.[83]

3.4 Processes in solid electrolyte membranes

The safe operation of solar-hydrogen systems requires that the produced gas streams have compositions below the flammability limit ($<4\%$ v/v of O_2 in H_2).[84,85] Despite some notable exceptions, the co-evolution of H_2 and O_2 in a common

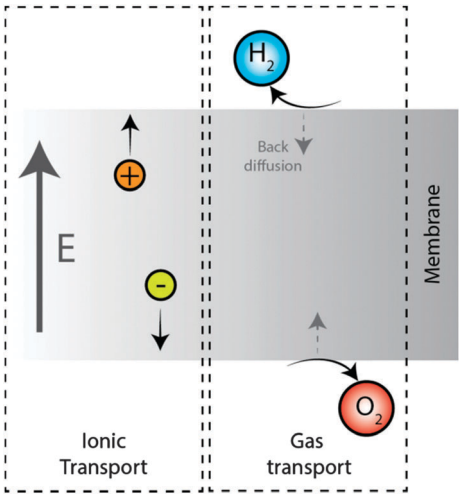

Fig. 8 Diagram of processes involved in the membrane. The balance between ion and gas transport directly affects the overall device performance.

electrolyte will usually lead to unsustainable levels of gas crossover.[83,86] To counteract this issue, membranes can be included in between reaction sites so that ionic conduction can be maintained between the hydrogen evolution side and the oxygen evolution side, while at the same time gas permeation can be averted (Fig. 8). These tasks are similar to those imposed in membranes used in fuel cell applications, although the ionic conduction and gas barrier requirements may differ. In general, the current density across the membrane depends on the material's conductivity, κ_{mem}, membrane thickness, L, and the ohmic potential drop across the membrane, $\nabla\phi_{mem}$,

$$j_{mem} = \kappa_{mem}\nabla\phi_{mem} \quad (14)$$

The gas crossover can be expressed in terms of a current equivalent loss, j_{XO}, which depends on the gas permeability for H_2 or O_2, ψ_{H_2} and ψ_{O_2} respectively, and the difference in partial pressures, p_{H_2/O_2}, between each side of the membrane,

$$j_{XO,H_2} = -n_{H_2}F\psi_{H_2}\nabla p_{H_2} \quad (15)$$

$$j_{XO,O_2} = n_{O_2}F\psi_{O_2}\nabla p_{O_2} \quad (16)$$

The values of j_{XO} can be used to estimate the losses in the electrodes arising from parasitic H_2 oxidation or O_2 reduction at the anode and cathode respectively, as it describes the current losses if all of the gas that back diffuses across the membrane is consumed at the electrodes. Furthermore, the ohmic and gas crossover energy losses can be derived as,

$$E_{ohm} = \frac{j^2 L}{\kappa} \quad (17)$$

$$E_{XO} = \sum_{i=H_2,O_2} |\psi_i \nabla p_i n_i F| E^0 \quad (18)$$

with E^0 being the standard potential for the water splitting reaction. These expressions describe the trade-off between the membrane ionic conduction and gas crossover encountered in membrane design. Moreover, they explicitly describe the factors that define the optimal membrane thickness, L_{op}, which results into minimal energy losses.

$$L_{op} = \left(\frac{FE^0}{j^2}\kappa \sum_{i=H_2,O_2} |\psi_i \nabla p_i n_i|\right)^{\frac{1}{2}} \quad (19)$$

The expression above can allow for an optimal membrane design given a set of device operating conditions. Also, this suggests that improved membrane materials should be designed so that the product between κ and ψ is minimized. Having introduced the main membrane design rules, we will summarize the state of the art membrane materials for solar water-splitting applications.

Perfluorinated sulfonic acid membranes. Fuel cell membranes based on perfluorinated sulfonic acid (PFSA) polymers, such as Nafion®, are often proposed and incorporated as suitable membranes for solar-hydrogen devices.[87–92] Nafion's remarkable ionic conductivity and gas blocking properties have made it the benchmark proton exchange membrane (PEM) material for ion-conduction application.[93,94] Additionally to finding applications in fuel cells, Nafion have also had an important impact in electrolysis. PEM electrolyzers are operated with only water as the feed (liquid electrolytes are not needed) and can reach high current densities (>5 A cm^{-2}) at high efficiencies ($>60\%$).[67] Furthermore, hydrogen can be compressed within the electrochemical cell, the electrolyzers can accommodate fluctuating power inputs, and can produce hydrogen at high levels of purity.[2,67,95–97] These desirable attributes make PEM water-splitting systems a promising technology for large scale implementation of hydrogen production systems.[98,99] While there are significant parallels between the membrane requirements in PEM electrolyzers and those in solar-hydrogen devices, there are still important distinctions that could drive the materials development apart. Mainly, optimized membranes depend on the operating current density of the system as described in eqn (19), and while PEM electrolyzer systems operate in the A cm^{-2} range, solar-hydrogen generator current densities can range between a few mA cm^{-2} to 100's of mA cm^{-2}. These current density differences lead to variations in the requirements for the membrane design. Considering typical proton conductivity[100] and gas permeability[101,102] properties of Nafion, the optimal membrane thicknesses for 10 mA cm^{-2} or 1 A cm^{-2} will vary from 10^3 μm to 10 μm (Fig. 9). This suggests that membranes with lower gas permeability can significantly help improve the efficiency and practical implementation of devices operated at low current density. Improving by a factor of 10 the gas barrier properties of Nafion for devices operated at current densities at 10 mA cm^{-2}, could bring the optimal thickness to the more suitable range of $\sim$320 μm.

To a limited extent these improvements can be achieved in Nafion membranes by controlling the internal structure of the material. Nafion's nanostructure is composed by ion-conducting domains embedded in a semi-crystalline matrix.[74,77,93,103–106] By increasing the crystallinity of the matrix, the permeability of the membrane can be decreased.[107] This is achieved by two internal changes: an increased tortuosity due to increased

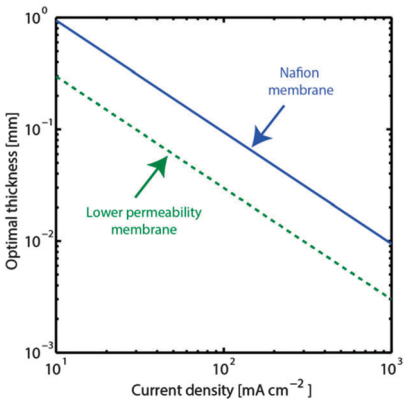

Fig. 9 Variation in optimal thickness as a function of current density imposed through the membrane. Nafion membranes with κ = 10 S m^{-1}, and ψ = 1.6 × 10^{-9} and 1.05 × 10^{-9} mol cm^{-1} s^{-1} bar^{-1} for H_2 and O_2 respectively. If the membrane thickness is improved by a factor of 10 (green dotted line) the optimal thickness can be reduced by a factor of $\sqrt{10}$.

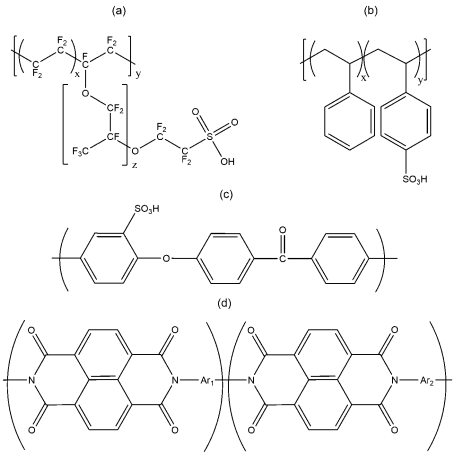

Fig. 10 Chemical structure of various PEM materials: (a) Nafion, (b) sulfonated polystyrene, (c) sulfonated polyether ether ketone and (d) polyimide-based membrane where Ar_1 and Ar_2 are arylene groups usually substituted with sulfonic acid groups that impart proton conductivity functionality.

volume fraction of crystallites, and a reduced water uptake of the ionic domains due to the stiffening of the surrounding matrix. It is important to point out that although these morphological changes might improve the gas barrier properties of the material, they will also affect the ionic conductivity which is tightly bound to the water content of the membrane. A more flexible strategy would involve the rational design of membranes with balanced ion-conduction and gas permeability. Other commercial membranes closely related to Nafion can provide additional tunability of the structure and length of the perfluorosulphonic acid side chains which could further help balance the transport properties of PFSA membranes.[108,109]

Alternative proton exchange membranes. While the PFSA membranes described above can enable a variety of early-stage solar-hydrogen devices, several shortcomings can hinder their large scale implementations. PFSA membranes require complex synthetic methods that result in large costs of production. Their chemical structures are fairly inflexible which impedes the exploration of membranes with balanced ionic conductivity and gas permeability. Moreover, the microstructure of PFSA membranes strongly depends on the processing properties of the material, which limits the study of the fundamental driving forces that lead to their desirable transport properties. These obstacles have motivated the investigation of polymer systems with higher degree of control over their chemical structure and morphology. Apart from the ionic and gas transport requirements, solar-fuel membranes need to be mechanically and electrochemically robust,[110] they need to have high permselectivity towards proton conduction, and they need to operate stably under aqueous environments (including strong electrolytes).

Based on those considerations, many research groups have developed polymeric systems that can serve as an alternative to PFSA PEM membranes.[111,112] Despite that the focus of these novel polymer membranes have been to substitute Nafion in fuel cell applications, their tunability can make them an attractive option for solar-hydrogen devices. Among the most researched alternative material figure aliphatic-backbone polymer systems, poly(arylene ether)-based membranes, and polyimide-based membranes (Fig. 10). Within the first class of membranes, sulfonated polystyrene membranes have been widely studied thanks to their well-developed simple synthesis and functionalization methods. One of the main limitations of these materials is the poor oxidative stability of the backbone which leads to membrane degradation during electrochemical operations. One of the main strategies to improve their stability involves the fluorination of the backbone which avoids the formation of hydroperoxide radicals and prevents the decay of the membranes. Other strategies involve crosslinking the polymer chains or incorporating radical trapping agents to minimize the degradation of the material.[113,114] Poly(arylene ether)-based membranes are also interesting systems because of their higher chemical, thermal and mechanical stability.[115] Among this group of polymers, sulfonated poly(ether ether ketone) (SPEEK) is the most widely studied system. Despite the advantages of these polymers, their long-term stability lags behind that of perfluorinated polymers and limits their practical implementation. Polyimide based polymers are also an attractive alternative as their conductivity is comparable to that of Nafion and they exhibit low gas permeability. Unfortunately, their implementation has also been limited due to their degradation through hydrolysis processes in the presence of water at elevated temperatures.

As described in the examples above, achieving stable proton exchange membranes that can operate in electrochemical devices for prolonged periods of times have proved to be a challenge and PFSA membranes remain to be the benchmark for PEMs. None-the-less efforts at improving the performance of alternative membrane materials could open up a broader range of possibilities for solar-fuel membranes.

Anion exchange membranes. While the field of PEMs is fairly well developed, anion exchange membranes (AEMs) are interesting alternatives for solar-fuels devices as they would allow the operation of systems under alkaline conditions. Operating water-splitting systems under alkaline conditions

have several advantages as it opens up the space for the incorporation of Ni based catalysts commonly used in alkaline electrolysis.[116–119] Commercial alkaline electrolyzers usually incorporate a porous diaphragm which provides limited gas separation capabilities while allowing hydroxide ions (OH^-) to be transported across electrodes. As these porous separators are highly permeable to gases, it is necessary that electrodes are placed much farther apart than in the case of PFSA electrolyzers. This has driven the development of AEMs towards systems with improved gas barrier properties while allowing OH^- ions to migrate with little resistance. Commercial AEMs are available from Tokuyama (now Astom Corporation) and Fumatech and they have found applications in water-splitting and fuel-cell systems.[120–126] These commercial membranes have conductivities in the order of 10 mS cm^{-1}, just one order of magnitude below the levels reachable by PFSA membranes. Given this performance level, their implementation in solar-hydrogen generators can be feasible, especially within those devices that require ionic currents in the order of 10 mA cm^{-2}. A few examples of promising solar-hydrogen systems that operate under basic environments have been demonstrated,[55,127–131] but only a few studies have incorporated anion exchange membranes or any mechanism to prevent gas crossover.[130,131]

As in the case of PEMs, alternative AEMs are attractive as they can lead to membrane materials with controllable levels of ionic and gas transport. Recent reviews have extensively covered the progress on these materials for electrochemical applications.[132–134] The most common polymeric AEMs are designed with positively charged side groups, based on either quaternary ammonium, imidazolium, pyridinium or quaternary phosphonium groups (Fig. 11). All of these systems suffer from poor stability under the required alkaline conditions. Multiple degradation mechanisms lead to loss of performance and failure in these systems. In the case of quaternized ammonium groups, the charged groups can undergo direct nucleophilic displacement. Also, if the polymer contains alkyl substituents with hydrogen atoms in the β position, degradation can occur *via* a Hofmann elimination mechanism. Implementing heterocyclic side groups such as pyridinium or imidazoliums ions can help alleviate these stability issues, but if H-substituents are present in the ring they can be attacked by OH^- ions ultimately leading to ring opening.[135] Alternatively to the nitrogen-based systems, phosphonium side groups can help improve the thermal stability of the materials, and at the same time lead to higher conductivities.[136,137] The stability constraints described above include the main mechanisms of degradation of functional side-groups in the presence of highly reactive OH^- ions. To some extent some AEMs can be operated for prolonged periods of time if the membranes are kept hydrated. As the water content in the AEMs decrease, the polymer degradation process accelerates leading to premature failure. Although this is a significant problem for AEMs used for fuel cell applications, in the case of solar-hydrogen generators the membranes are expected to be fully immersed in water for the lifetime of the device. Also, additionally to the stability concerns of charged side groups, degradation of the backbone should be considered for long term stability. The problem of backbone degradation in AEMs is not unique to alkaline systems, as the same processes are evidenced in PEMs. In the case of systems operated under strongly basic conditions, degradation mediated by $OH^{\bullet}$ radical is the most concerning mechanism.[138,139]

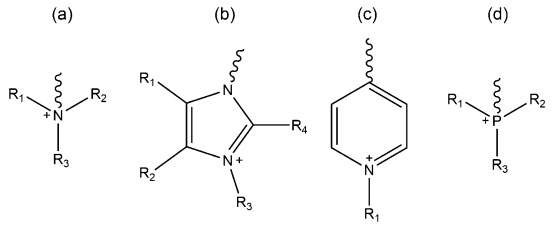

Fig. 11 Commonly used charged side-groups for polymeric AEMs: (a) quaternary amines, (b) imidazolium, (c) pyridinium, (d) quaternary phosphonium ions.

Evidently, the development of AEMs lags behind their proton conducting counterparts, both in terms of reliability and conductivity. Significant challenges preclude AEMs membranes from operating with resistance and stability levels similar to PEMs, which has motivated a rich field of research around understanding and providing solutions to many of these issues. AEMs will certainly play a key role in solar-hydrogen generators as many of the semiconductor or catalyst materials are stable (or can be stabilized) under basic conditions. Furthermore, AEMs in conjunction with PEMs – *i.e.* bipolar membranes – can enable devices where the oxidation and reduction sides operate under different pH regimes.[140–143] Bipolar membrane devices where the AEMs are in contact with a basic solution and the PEM side is in contact with an acidic solution, can allow for the incorporation of acid-stable HER catalysts and base-stable OER catalysts within the same system. Moreover, as water molecules split into H^+ and OH^- ions at the interface between the AEM and PEM, the steady state current density in the device can be carried by these ions exclusively, avoiding the depletion of supporting ions. The added flexibility provided by bipolar membranes can enable the incorporation of photo-catalytic material pairs (OER and HER) under otherwise incompatible pH conditions.

Block-copolymer strategies for ion-conducting membranes. In the previous sub-sections we stressed that achieving a balance between ionic and gas transport properties could broaden the range of operating conditions of solar-hydrogen generators. In this regard, block-copolymer (BCP) membranes could provide an additional handle to achieve the desired balance. Specifically, a block-copolymer strategy can allow for the incorporation of ion-conducting domains together with good gas barrier and structurally stable domains (Fig. 12). As the transport properties of each of the involved species could be modulated by the volume fractions of the blocks, a broader range of transport properties combinations can be achieved. Furthermore, BCPs allow for a precise control on the internal morphology of the membranes, so that different levels of tortuosity and connectivity in between domains can be achieved.[144,145] Similar strategies have been already implemented in membranes for fuel-cell applications.[146] This type of membranes can incorporate a broad range of ion-conducting groups such as the ones described in the

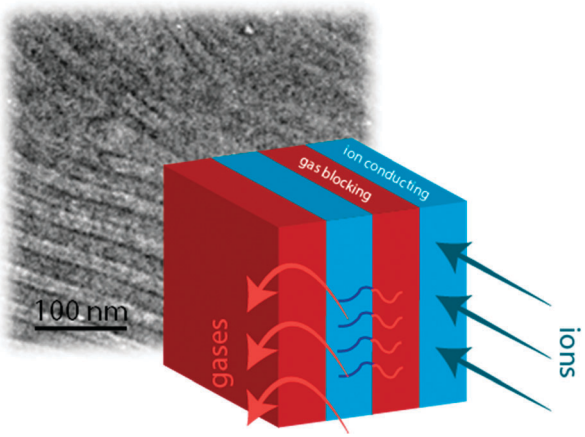

Fig. 12 Schematic representation of block-copolymer membranes showing a lamellar morphology. Ions are transported through ion-conducting domains, while gas blocking domains provide structural support and prevent gas crossover. The TEM image shown in the back corresponds to a lamellar BCP based PEM.[148]

alternative PEM[147–158] or AEM[159–163] sections above. Alternatively, BCP can be designed so that one of the domains selectively contains electrolytes such as ionic liquids; in this way enjoying the morphological level of control provided by BCP and the high-ionic conductivity of liquid electrolytes.[164–169] It must be noted that such systems can suffer from electrolyte leakage if operated under liquid environments, so their implementation might be more appropriate for devices operated with water vapor feeds.

In terms of the gas barrier blocks, polymers with high level of crystallinity, high glass transition temperatures, and/or low free volume could be incorporated to reduce gas crossover. Some promising gas barrier blocks include: semi-crystalline polyethylene, hydrogenated polystyrene, polyacrylamide, among others. Additionally, block-copolymer membranes can exhibit unconventional properties due to the spatial confinement of conducting domains. Some notable examples include membranes that uptake higher levels of water due to capillary condensation in conducting domains below 5 nm.[170,171] Also, the behavior of conducting polymer chains near the interface between conducting and structural domains can be significantly different than the bulk behavior. This is due to the decreased mobility arising from chain confinement at the interface which can lead to lower water uptake and ultimately affect the ionic conductivity.[172,173] The rich behavior of BCP membranes makes them an interesting model system that can help elucidate the transport mechanism of ionic-conducting membranes. Developing the design rules required for conducting BCP membranes can lead to materials with high level of control over the transport properties of the multiple species involved in solar-hydrogen generators.

4. Coupled processes in integrated solar-hydrogen devices

Functional solar hydrogen devices require the coupled operation of the multiple transport processes described in the previous sections. The performance of an integrated device will depend on the interplay of all of these processes, and the rates at which they occur will ultimately dictate the hydrogen production rate and solar to hydrogen conversion efficiency. While this review describes a basic set of equations that govern each of the processes involved, the solution to them in a real device configuration is challenging due to the coupling of multi-physics processes that occur at very different length and time scales. Recent studies have attempted to numerically describe the operation of integrated devices with generalized configurations. Berger and Newman developed a detailed 1-dimensional model that accounted for light absorption, charge generation and separation, charge transport across the semiconductor–metal interface, electrochemical reaction at the metal catalysts, and ion transport within the electrolyte.[174] Gaudy and Haussener extended this model by incorporating the detailed solution of the Maxwell equations to account for complex morphological heterogeneities in the absorber, and by providing a detailed model for surface state un/pinning at the direct semiconductor–electrolyte interface.[175] Haussener *et al.* analysed the interplay between the electro kinetics and ionic transport in a set of 2-dimensional device configurations; leading to a better understanding on the current density distribution across electrode systems and the effects of temperature variations on device performance.[83,176] Tembhurne *et al.* developed a complete 2-dimensional PEC device model specifically accounting for the detailed energy balance in the various components requiring a complex solution procedure with multiple local and global iteration loops to properly account for the temperature effect in the charge conservation equations. This model is the most complete and detailed macroscopic PEC model to date.[177] Several groups have started to model different device configurations and operating conditions leading to optimized device designs.[82,89] Notably, modelling of transport processes has provided insights into the design of solar-water splitting devices operated under water vapor feeds,[65,178,179] and near-neutral pH electrolytes.[43,82] These conditions have complex mass transport characteristics due to the limitations expected from the low concentration of water in vapor feeds, or the presence of multiple ionic species with non-uniform concentrations in buffered electrolytes.

Experimental implementations of solar-hydrogen devices spam a wide range of device architectures and functional materials.[15,180,181] Architectures where photovoltaics are electrically coupled with electrolysis units can be implemented with commercially available components.[92,182–187] Within this configuration, the light absorber is not in contact with the electrolyte, and the system can be optimized so that the current output from the PV component matches that of the electrolysis units (Fig. 13(a)).[188] State of the art electrolyzers are based on nanostructured catalysts layers separated by proton exchange membranes such as Nafion. In these devices, transport of water and product gases depends on the structure and material properties of the catalysts layer components, while ion transport occurs through the thickness of the PEM (usually <100 μm) and the ionomer binder used in catalysts layers. A higher level of integration can be achieved if the light absorption and electrocatalytic

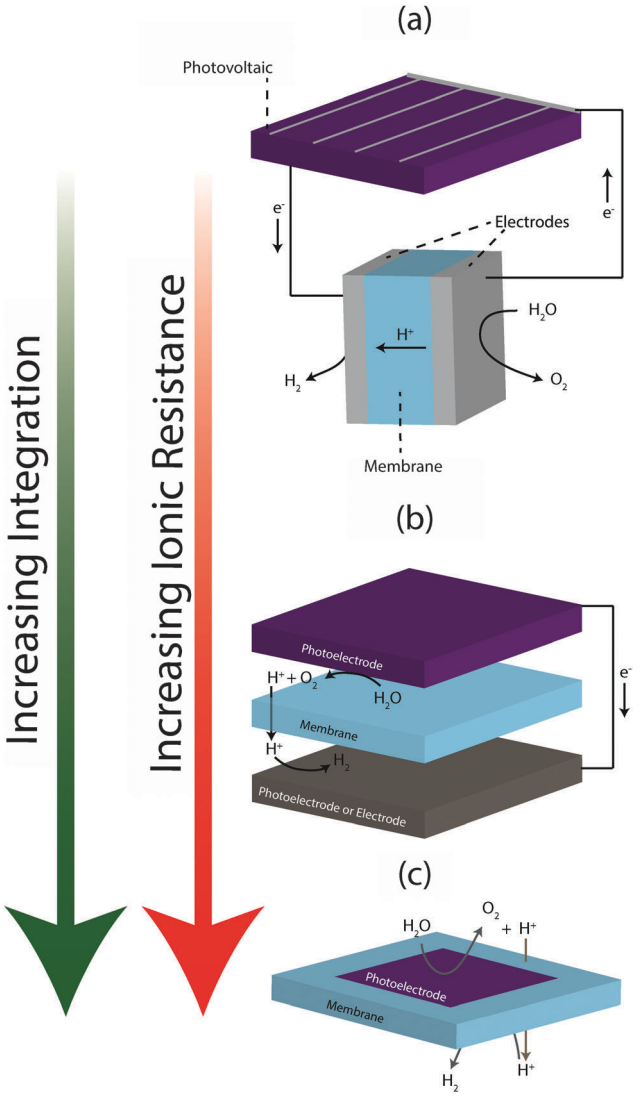

Fig. 13 Various integrated device configurations: (a) photovoltaic arrays electrically coupled with a PEM electrolyzer, (b) two electrode devices based on at least one photoelectrode, and (c) monolithically integrated wireless solar-hydrogen generation system.

functionality is combined in a single photoelectrode. Devices based on photo-electrodes can be divided into wired two electrode devices or monolithically integrated wireless devices (Fig. 13(b) and (c) respectively). Two electrode systems involving at least one photoelectrode have been demonstrated extensively in the literature.[52,59,64,82,128–130,189–192] Within this configuration, the ionic resistance in the system can be minimized by reducing the inter-electrode distance. Only a few examples of wireless devices have been demonstrated.[59,193,194] The ionic resistance in these systems tends to be higher than in the two other device types described above, as the ionic charge carriers need two migrate laterally across the surface of the semiconductor, and then transversally across an ion-conductor.[195] The long pathways for migration can result in current density asymmetries in the surface of the (photo)electrodes[83] ultimately resulting in higher ohmic losses. To mitigate these limitations, photoelectrodes can be designed in the microscale (*e.g.* microwires embedded into ion-conducting membranes[54,196,197]) so that the lateral migration of ionic species is mainly dictated by distance between the reaction sites at opposite ends of the microstructures. The generalized discussion presented above summarizes some of the design principles for three prominent architectures of solar-hydrogen generators. For a more detailed assessment on design, fabrication and operation aspects of integrated devices, readers are referred to a recent literature review.[5]

5. Conclusions and perspectives

Throughout this review we described thoroughly the progress on the engineering aspects of integrated solar-hydrogen generators. By doing so, we not only provided a snapshot of the state-of-the-art in the development of particular components leading to full devices, but also lay the foundations that guide the design of optimal solar-hydrogen systems. Deliberately, this article treats the aspects of light-absorption and electrocatalysis superficially, as most of the focus in the past has been given to the development of these components. Instead, the angle taken in this review considers those processes as boundary phenomena that define the conditions and requirements that the transport processes within the device will need to accommodate. The description provided for the light-absorption and electrocatalysis processes should guide the reader towards understanding how these components interact with the rest of the device. By focusing on the transport processes, we have tackled the design questions that define the ionic conduction, product separation and collection aspects required for a fully functioning device.

As described in the sections above, three critical regions were identified which interact with each other and ultimately define the device performance: the boundary layer, the bulk electrolyte, and the membrane. The boundary layer region is often overlooked, but a closer attention should be given to it as it generally defines the performance limitation of the devices. The transport processes within this region are dominated by diffusion of reactive or ionic species into and from the catalytic surface. Depending on the electrolyte composition this region can lead to diffusion limited current densities, especially if the device is operated under buffered electrolytes at moderate pH conditions. Whenever possible, devices should be operated under strong acidic or basic electrolytes. This would alleviate transport limitations and the formation of large concentration gradients in the boundary layer, as well as to accelerate the catalysis processes in the electrodes due to the increased concentration of reactive intermediates (H^+ or OH^-). On the other hand, it is well accepted that a large number of semiconductor or catalyst materials are not stable under these corrosive environments. In those cases, it is highly desirable to develop approaches where near-neutral buffered solutions are implemented as the electrolyte. These approaches should mitigate the formation of pH gradients around the surface of the electrodes. Flow based systems are a promising alternative in these cases, as the introduced convection can be used to reduce the size of the

diffusion boundary layer, and in this way accelerate the transport of H^+ or OH^- species. Research in this area can provide insights into the transport of multi-ion buffered electrochemical systems and could lead to the development of processes to operate solar-hydrogen generators under near-neutral conditions at high current densities. Some modelling efforts have started to analyse buffered systems under a set of limited conditions (*i.e.* passive systems, or flow systems at low Re numbers), providing important insights into the performance limits of devices operated at near-neutral pH.[43] Experimental and theoretical investigations that expand upon this area and are geared towards describing solutions to the pre-existing problems of buffered electrolyte systems could positively impact the solar-fuels field by enabling material systems that are only stable under mild pH conditions.

Critical transport processes in the bulk electrolyte involve the transport of ionic species between electrodes and gases from the evolution sites to collection ports. To avoid significant ionic resistance losses, the design of reactor architectures should minimize the ionic path-length. This is particularly important for devices that operate at high current densities (>100 mA cm^{-2}) as the potential losses in the electrolyte can account for 100's mV. It is also important to keep in mind, that flow systems, such as the ones implemented in commercial fuel cell or electrolysis units, can alleviate the mass transport limitations of devices and aid in the collection of the fuel streams while mitigating gas crossover. To this end, stagnant cells or those where low flow rates are implemented will suffer from large gas back diffusion, and will most certainly require the implementation of membranes to avoid unallowable levels of oxygen contamination in the hydrogen fuel stream.

Membranes are likely to continue to be critical components in the development of solar-hydrogen generators. As suggested in this article, achieving a balance between high ionic conductivity and low gas permeability is the main challenge in the area of solar-fuels membranes. Research opportunities in different directions could lead to this desirable balance. Some of these opportunities can be found in the areas of block-copolymer membranes with multi-functional domains. Polymer blends can also be an interesting alternative, where conducting and gas impermeable materials are implemented to achieve balanced transport. Other promising solutions include the use of semi-crystalline ion-conducting polymer where the level of crystallinity defines the gas transport properties. Lastly, nanocomposite materials with ion conducting polymers and inorganic inclusions with low gas permeability can help achieve the desired balance.

Lastly, it is of the authors' opinion that the engineering design aspects discussed in this article as well as techno-economic and environmental feasibility analysis should be implemented early-on in the design of solar-hydrogen generators.[188,198–200] This approach can significantly accelerate the development of viable devices, and help direct research resources towards areas of large impact. This can also help to avoid future roadblocks or dead-end pathways that would fundamentally limit the implementation of solar-hydrogen technologies. Thanks to the basic-science developments of the photo-electrochemical scientific community in the past four decades we are placed in a privileged position to exploit the scientific achievements of the past and engineer solar-hydrogen systems that could help our world move towards cleaner fuels. This will only be possible under strong interdisciplinary R&D programs with the clear and unbiased goal of developing the technological foundations necessary for the implementation of solar-fuel generators.

Nomenclature

Latin symbols

c	Local concentration of carriers/species
C	Capacity of double layer
D	Diffusion coefficient of carriers/species
$\boldsymbol{E}$	Electric field vector
f	Function describing the electrode kinetics
F	Faraday's constant
G	Generation rate
$\boldsymbol{j}$	Net carrier flux/current density vector
j_0	Exchange current density
k	Mass transfer coefficient of species
K	Apparent permeability of the liquid through separator
L	Membrane thickness
$\hat{\boldsymbol{n}}$	Unit normal vector
n	Stoichiometric coefficient
$\boldsymbol{N}$	Molar flux vector
p	Pressure
R	Recombination rate/reaction source term/gas constant
Re	Reynolds number
Sh	Sherwood number
Sc	Schmidt number
t	Time
T	Temperature
$\boldsymbol{u}$	Velocity vector
u	Mobility of species
$\langle \boldsymbol{u} \rangle$	Superficial velocity vector
x	Characteristic length
z	Charge/valence

Greek symbols

α	Apparent transfer coefficient
δ_c	Mass transport boundary layer thickness
η	Electrode surface overpotential
ϕ	Potential
κ	Ionic conductivity
ρ	Density
ν	Kinematic viscosity
ε	Porosity
ψ	Gas permeability
μ	Mobility of charge carriers/dynamic viscosity
γ	Exponent in generalized Buttler–Volmer expression

Subscripts

a	Anodic
bulk	Bulk

c	Cathodic
e	Effective
i	Charge/species index
mem	Membrane
ox	Oxidation
red	Reduction
surf	surface
XO	Crossover

(Bolded letters and symbols represent vectorial quantities)

Acknowledgements

This material is based upon work performed with the financial support of the Nano-Tera.ch initiative, as part of the Solar Hydrogen Integrated Nano Electrolysis project (Grant # 530 101). The authors would like to thank Prof. Demetri Psaltis and Prof. Christophe Moser for useful discussions.

Notes and references

1 S. Chu and A. Majumdar, *Nature*, 2012, **488**, 294–303.
2 G. Saur and T. Ramsden, *Wind Electrolysis: Hydrogen Cost Optimization*, 2011.
3 N. S. Lewis and D. G. Nocera, *Proc. Natl. Acad. Sci. U. S. A.*, 2006, **103**, 15729–15735.
4 International Energy Agency Technology Roadmap, Energy Storage, 2014.
5 M. A. Modestino and S. Haussener, *Annu. Rev. Chem. Biomol. Eng.*, 2015, **6**, 13–34.
6 M. G. Walter, E. L. Warren, J. R. McKone, S. W. Boettcher, Q. Mi, E. A. Santori and N. S. Lewis, *Chem. Rev.*, 2010, **110**, 6446–6473.
7 L. J. Minggu, W. R. W. Daud and M. B. Kassim, *Int. J. Hydrogen Energy*, 2010, **35**, 5233–5244.
8 J. Q. Chen, D. H. Yang, D. Song, J. H. Jiang, A. B. Ma, M. Z. Hu and C. Y. Ni, *J. Power Sources*, 2015, **280**, 649–666.
9 D. Gust, T. A. Moore and A. L. Moore, *Acc. Chem. Res.*, 2009, **42**, 1890–1898.
10 K. Sivula, F. Le Formal and M. Gratzel, *ChemSusChem*, 2011, **4**, 432–449.
11 F. E. Osterloh, *Chem. Soc. Rev.*, 2013, **42**, 2294–2320.
12 Z. B. Chen, T. F. Jaramillo, T. G. Deutsch, A. Kleiman-Shwarsctein, A. J. Forman, N. Gaillard, R. Garland, K. Takanabe, C. Heske, M. Sunkara, E. W. McFarland, K. Domen, E. L. Miller, J. A. Turner and H. N. Dinh, *J. Mater. Res.*, 2010, **25**, 3–16.
13 T. Hisatomi, J. Kubota and K. Domen, *Chem. Soc. Rev.*, 2014, **43**, 7520–7535.
14 L. C. Seitz, Z. Chen, A. J. Forman, B. A. Pinaud, J. D. Benck and T. F. Jaramillo, *ChemSusChem*, 2014, **7**, 1372–1385.
15 J. W. Ager, M. R. Shaner, K. A. Walczak, I. D. Sharp and S. Ardo, *Energy Environ. Sci.*, 2015, **8**, 2811–2824.
16 M. A. Modestino and S. Haussener, *Annu. Rev. Chem. Biomol. Eng.*, 2013, **6**, 13–34.
17 D. K. Bora, A. Braun and E. C. Constable, *Energy Environ. Sci.*, 2013, **6**, 407–425.
18 X. Chen, S. Shen, L. Guo and S. S. Mao, *Chem. Rev.*, 2010, **110**, 6503–6570.
19 X. Chen and S. S. Mao, *Chem. Rev.*, 2007, **107**, 2891–2959.
20 E. Kemppainen, J. K. Halme and P. Lund, *J. Phys. Chem. C*, 2015, 21747–21766.
21 M. Modest, *Radiative Heat Transfer*, Academic Press, Waltham, MA, 2003.
22 M. I. Mishchenko, *Rev. Geophys.*, 2008, **46**, 1–33.
23 M. I. Mishchenko, V. P. Tishkovets, L. D. Travis, B. Cairns, J. M. Dlugach, L. Liu, V. K. Rosenbush and N. N. Kiselev, *J. Quant. Spectrosc. Radiat. Transfer*, 2011, **112**, 671–692.
24 K. T. Fountaine and H. A. Atwater, *Opt. Express*, 2014, **22**, A1453–A1461.
25 K. T. Fountaine, C. G. Kendall and H. A. Atwater, *Opt. Express*, 2014, **22**, A930–A940.
26 H. Doscher, J. F. Geisz, T. G. Deutsch and J. A. Turner, *Energy Environ. Sci.*, 2014, **7**, 2951–2956.
27 J. Newman and K. Thomas-Alyea, *Electrochemical Systems*, Wiley & Sons, 2004.
28 M. Gong and H. Dai, *Nano Res.*, 2015, **8**, 23–39.
29 F. Safizadeh, E. Ghali and G. Houlachi, *Int. J. Hydrogen Energy*, 2015, **40**, 256–274.
30 M. Hamdani, R. N. Singh and P. Chartier, *Int. J. Electrochem. Sci.*, 2010, **5**, 556–577.
31 J. Lee, B. Jeong and J. D. Ocon, *Curr. Appl. Phys.*, 2013, **13**, 309–321.
32 J. Kibsgaard, C. Tsai, K. Chan, J. D. Benck, J. K. Norskov, F. Abild-Pedersen and T. F. Jaramillo, *Energy Environ. Sci.*, 2015, 3022–3029.
33 C. C. L. McCrory, S. Jung, J. C. Peters and T. F. Jaramillo, *J. Am. Chem. Soc.*, 2013, **135**, 16977–16987.
34 C. C. McCrory, S. Jung, I. M. Ferrer, S. M. Chatman, J. C. Peters and T. F. Jaramillo, *J. Am. Chem. Soc.*, 2015, **137**, 4347–4357.
35 J. O'M. Bockris, B. E. Conway and E. Yeager, *The double layer*, Plenum press, New York, 1980.
36 B. B. Damaskin and O. A. Petrii, *J. Solid State Electrochem.*, 2011, **15**, 1317–1334.
37 D. A. Walker, B. Kowalczyk, M. O. de la Cruz and B. A. Grzybowski, *Nanoscale*, 2011, **3**, 1316–1344.
38 I. Llorente, S. Fajardo and J. M. Bastidas, *J. Solid State Electrochem.*, 2014, **18**, 293–307.
39 L. Joly, C. Ybert, E. Trizac and L. Bocquet, *Phys. Rev. Lett.*, 2004, **93**, 257805.
40 C. D. Taylor and M. Neurock, *Curr. Opin. Solid State Mater. Sci.*, 2005, **9**, 49–65.
41 E. L. Cussler, *Diffusion: Mass Transfer in Fluid Systems*, Cambridge University press, Cambridge, UK, 2003.
42 W. Deen, *Analysis of Transport Phenomena*, Oxford University Press, New York, 1998.
43 M. R. Singh, K. Papadantonakis, C. Xiang and N. S. Lewis, *Energy Environ. Sci.*, 2015, **8**, 2760–2767.
44 N. Papageorgiou, M. Gratzel and P. P. Infelta, *Sol. Energy Mater. Sol. Cells*, 1996, **44**, 405–438.

45 D. V. Esposito, J. B. Baxter, J. John, N. Lewis, T. P. Moffat, T. Ogitsu, G. D. O'Neil, T. A. Pham, A. A. Talin, J. M. Velazquez and B. Wood, *Energy Environ. Sci.*, 2015, 2863–2885.
46 A. J. Bard and M. V. Mirkin, *Scanning electrochemical microscopy*, CRC Press, 2012.
47 B. R. Horrocks, M. V. Mirkin, D. T. Pierce, A. J. Bard, G. Nagy and K. Toth, *Anal. Chem.*, 1993, **65**, 1213–1224.
48 M. Etienne, P. Dierkes, T. Erichsen, W. Schuhmann and I. Fritsch, *Electroanalysis*, 2007, **19**, 318–323.
49 Y. F. Yang and G. Denuault, *J. Chem. Soc., Faraday Trans.*, 1996, **92**, 3791–3798.
50 A. J. Leenheer and H. A. Atwater, *J. Electrochem. Soc.*, 2012, **159**, H752–H757.
51 S. M. H. Hashemi, M. A. Modestino and D. Psaltis, *Energy Environ. Sci.*, 2015, **8**, 2003–2009.
52 O. Khaselev and J. A. Turner, *Science*, 1998, **280**, 425–427.
53 K. Walczak, Y. K. Chen, C. Karp, J. W. Beeman, M. Shaner, J. Spurgeon, I. D. Sharp, X. Amashukeli, W. West, J. Jin, N. S. Lewis and C. X. Xiang, *ChemSusChem*, 2015, **8**, 544–551.
54 M. R. Shaner, J. R. McKone, H. B. Gray and N. S. Lewis, *Energy Environ. Sci.*, 2015, 2977–2984.
55 S. A. Bonke, M. Wiechen, D. R. MacFarlane and L. Spiccia, *Energy Environ. Sci.*, 2015, **8**, 2791–2796.
56 C. Y. Lin, Y. H. Lai, D. Mersch and E. Reisner, *Chem. Sci.*, 2012, **3**, 3482–3487.
57 P. Bornoz, F. F. Abdi, S. D. Tilley, B. Dam, R. van de Krol, M. Graetzel and K. Sivula, *J. Phys. Chem. C*, 2014, **118**, 16959–16966.
58 J. S. Luo, J. H. Im, M. T. Mayer, M. Schreier, M. K. Nazeeruddin, N. G. Park, S. D. Tilley, H. J. Fan and M. Gratzel, *Science*, 2014, **345**, 1593–1596.
59 S. Y. Reece, J. A. Hamel, K. Sung, T. D. Jarvi, A. J. Esswein, J. J. H. Pijpers and D. G. Nocera, *Science*, 2011, **334**, 645–648.
60 C. R. Cox, J. Z. Lee, D. G. Nocera and T. Buonassisi, *Proc. Natl. Acad. Sci. U. S. A.*, 2014, **111**, 14057–14061.
61 J. H. Park, S. Kim and A. J. Bard, *Nano Lett.*, 2006, **6**, 24–28.
62 C. Liu, J. Y. Tang, H. M. Chen, B. Liu and P. D. Yang, *Nano Lett.*, 2013, **13**, 2989–2992.
63 J. Brillet, J. H. Yum, M. Cornuz, T. Hisatomi, R. Solarska, J. Augustynski, M. Graetzel and K. Sivula, *Nat. Photonics*, 2012, **6**, 823–827.
64 F. F. Abdi, L. H. Han, A. H. M. Smets, M. Zeman, B. Dam and R. van de Krol, *Nat. Commun.*, 2013, **4**, 2195.
65 M. A. Modestino, M. Dumortier, M. Hashemi, S. Haussener, C. Moser and D. Psaltis, *Lab Chip*, 2015, **15**, 2287–2296.
66 J. M. Spurgeon and N. S. Lewis, *Energy Environ. Sci.*, 2011, **4**, 2993–2998.
67 M. Carmo, D. L. Fritz, J. Mergel and D. Stolten, *Int. J. Hydrogen Energy*, 2013, **38**, 4901–4934.
68 T. Soboleva, K. Malek, Z. Xie, T. Navessin and S. Holdcroft, *ACS Appl. Mater. Interfaces*, 2011, **3**, 1827–1837.
69 M. K. Debe, *ECS Trans.*, 2012, **45**, 47–68.
70 M. K. Debe, S. M. Maier-Hendricks, G. Vernstrom, J. Willey, M. Hamden, C. K. Mittelsteadt, C. Capuano, K. E. Ayers and E. Anderson, *ECS Meeting Abstracts*, 2011, **MA2011–02**, 694.
71 M. A. Modestino, D. K. Paul, S. Dishari, S. A. Petrina, F. I. Allen, M. A. Hickner, K. Karan, R. A. Segalman and A. Z. Weber, *Macromolecules*, 2013, **46**, 867–873.
72 M. A. Modestino, A. Kusoglu, A. Hexemer, A. Z. Weber and R. A. Segalman, *Macromolecules*, 2012, **45**, 4681–4688.
73 S. A. Eastman, S. Kim, K. A. Page, B. W. Rowe, S. Kang, C. L. Soles and K. G. Yager, *Macromolecules*, 2012, **45**, 7920–7930.
74 M. Bass, A. Berman, A. Singh, O. Konovalov and V. Freger, *Macromolecules*, 2011, **44**, 2893–2899.
75 D. K. Paul, A. Fraser and K. Karan, *Electrochem. Commun.*, 2011, **13**, 774–777.
76 A. Kusoglu, D. Kushner, D. K. Paul, K. Karan, M. A. Hickner and A. Z. Weber, *Adv. Funct. Mater.*, 2014, **24**, 4763–4774.
77 F. Allen, L. Comoli, A. Kusoglu, M. A. Modestino, A. Minor and A. Z. Weber, *ACS Macro Lett.*, 2015, **4**, 1–5.
78 J. Ronge, S. Deng, S. Pulinthanathu Sree, T. Bosserez, S. W. Verbruggen, N. Kumar Singh, J. Dendooven, M. B. J. Roeffaers, F. Taulelle, M. De Volder, C. Detavernier and J. A. Martens, *RSC Adv.*, 2014, **4**, 29286–29290.
79 M. A. Modestino, C. A. Diaz-Botia, S. Haussener, R. Gomez-Sjoberg, J. W. Ager and R. A. Segalman, *Phys. Chem. Chem. Phys.*, 2013, **15**, 7050–7054.
80 A. Dukic and M. Firak, *Int. J. Hydrogen Energy*, 2011, **36**, 7799–7806.
81 E. A. Hernandez-Pagan, N. M. Vargas-Barbosa, T. H. Wang, Y. X. Zhao, E. S. Smotkin and T. E. Mallouk, *Energy Environ. Sci.*, 2012, **5**, 7582–7589.
82 M. A. Modestino, K. A. Walczak, A. Berger, C. M. Evans, S. Haussener, C. Koval, J. S. Newman, J. W. Ager and R. A. Segalman, *Energy Environ. Sci.*, 2014, **7**, 297–301.
83 S. Haussener, C. X. Xiang, J. M. Spurgeon, S. Ardo, N. S. Lewis and A. Z. Weber, *Energy Environ. Sci.*, 2012, **5**, 9922–9935.
84 H. F. Coward and G. W. Jones, *Limits of flammability of gases and vapors*, Bureau of Mines, Washington, DC, 1952.
85 H. Le, S. Nayak and M. S. Mannan, *Ind. Eng. Chem. Res.*, 2012, **51**, 9396–9402.
86 J. Jin, K. Walczak, M. R. Singh, C. Karp, N. S. Lewis and C. Xiang, *Energy Environ. Sci.*, 2014, **7**, 3371–3380.
87 M. A. Modestino and R. A. Segalman, *Bridge on Frontiers of Engineering*, 2013, **43**, 23–30.
88 B. Seger and P. V. Kamat, *J. Phys. Chem. C*, 2009, **113**, 18946–18952.
89 K. Walczak, Y. Chen, C. Karp, J. W. Beeman, M. Shaner, J. Spurgeon, I. D. Sharp, X. Amashukeli, W. West, J. Jin, N. S. Lewis and C. Xiang, *ChemSusChem*, 2015, **8**, 544–551.
90 J. W. Ager Iii, M. Shaner, K. Walczak, I. D. Sharp and S. Ardo, *Energy Environ. Sci.*, 2015, **8**, 2811–2824.
91 J. M. Spurgeon, M. G. Walter, J. Zhou, P. A. Kohl and N. S. Lewis, *Energy Environ. Sci.*, 2011, **4**, 1772–1780.

92 G. Peharz, F. Dimroth and U. Wittstadt, *Int. J. Hydrogen Energy*, 2007, **32**, 3248–3252.
93 K. A. Mauritz and R. B. Moore, *Chem. Rev.*, 2004, **104**, 4535–4585.
94 J. S. Chiou and D. R. Paul, *Ind. Eng. Chem. Res.*, 1988, **27**, 2161–2164.
95 H. Ito, T. Maeda, A. Nakano and H. Takenaka, *Int. J. Hydrogen Energy*, 2011, **36**, 10527–10540.
96 M. Schalenbach, M. Carmo, D. L. Fritz, J. Mergel and D. Stolten, *Int. J. Hydrogen Energy*, 2013, **38**, 14921–14933.
97 M. K. Debe, A. J. Steinbach and K. Noda, *ECS Trans.*, 2006, **3**, 835–853.
98 N. Independent Review Panel, Current (2009) State-of-the-Art Hydrogen Production Cost Estimate Using Water Electrolysis, 2009.
99 K. E. Ayers, E. B. Anderson, C. Capuano, B. Carter, L. Dalton, G. Hanlon, J. Manco and M. Niedzwiecki, *ECS Trans.*, 2010, **33**, 3–15.
100 T. A. Zawodzinski, C. Derouin, S. Radzinski, R. J. Sherman, V. T. Smith, T. E. Springer and S. Gottesfeld, *J. Electrochem. Soc.*, 1993, **140**, 1041–1047.
101 A. Z. Weber and J. Newman, *J. Electrochem. Soc.*, 2004, **151**, 311–325.
102 A. Berger, R. A. Segalman and J. Newman, *Energy Environ. Sci.*, 2014, **7**, 1468–1476.
103 K. Schmidt-Rohr and Q. Chen, *Nat. Mater.*, 2008, **7**, 75–83.
104 G. Gebel, *Polymer*, 2000, **41**, 5829–5838.
105 T. D. Gierke, G. E. Munn and F. C. Wilson, *J. Polym. Sci., Polym. Phys. Ed.*, 1981, **19**, 1687–1704.
106 L. Rubatat, A. L. Rollet, G. Gebel and O. Diat, *Macromolecules*, 2002, **35**, 4050–4055.
107 C. M. Evans, M. R. Singh, N. A. Lynd and R. A. Segalman, *Macromolecules*, 2015, **48**, 3303–3309.
108 D. Wu, S. J. Paddison, J. A. Elliott and S. J. Hamrock, *Langmuir*, 2010, **26**, 14308–14315.
109 S. J. Hamrock and A. M. Herring, *Fuel Cells*, Springer, 2013, pp. 577–605.
110 R. Borup, J. Meyers, B. Pivovar, Y. S. Kim, R. Mukundan, N. Garland, D. Myers, M. Wilson, F. Garzon, D. Wood, P. Zelenay, K. More, K. Stroh, T. Zawodzinski, J. Boncella, J. E. McGrath, M. Inaba, K. Miyatake, M. Hori, K. Ota, Z. Ogumi, S. Miyata, A. Nishikata, Z. Siroma, Y. Uchimoto, K. Yasuda, K.-I. Kimijima and N. Iwashita, *Chem. Rev.*, 2007, **107**, 3904–3951.
111 H. Zhang and P. K. Shen, *Chem. Rev.*, 2012, **112**, 2780–2832.
112 M. A. Hickner, H. Ghassemi, Y. S. Kim, B. R. Einsla and J. E. McGrath, *Chem. Rev.*, 2004, **104**, 4587–4612.
113 C.-A. Dai, C.-P. Liu, Y.-H. Lee, C.-J. Chang, C.-Y. Chao and Y.-Y. Cheng, *J. Power Sources*, 2008, **177**, 262–272.
114 S. Saga, H. Matsumoto, K. Saito, M. Minagawa and A. Tanioka, *J. Power Sources*, 2008, **176**, 16–22.
115 G. Maier and J. Meier-Haack, *Fuel cells II*, Springer, 2008, pp. 1–62.
116 K. Zeng and D. Zhang, *Prog. Energy Combust. Sci.*, 2010, **36**, 307–326.
117 R. L. LeRoy, *Int. J. Hydrogen Energy*, 1983, **8**, 401–417.
118 Y. Leng, G. Chen, A. J. Mendoza, T. B. Tighe, M. A. Hickner and C.-Y. Wang, *J. Am. Chem. Soc.*, 2012, **134**, 9054–9057.
119 G. Merle, M. Wessling and K. Nijmeijer, *J. Membr. Sci.*, 2011, **377**, 1–35.
120 M. Carmo, G. Doubek, R. C. Sekol, M. Linardi and A. D. Taylor, *J. Power Sources*, 2013, **230**, 169–175.
121 K. Matsuoka, Y. Iriyama, T. Abe, M. Matsuoka and Z. Ogumi, *J. Power Sources*, 2005, **150**, 27–31.
122 J. R. Varcoe, M. Beillard, D. M. Halepoto, J. P. Kizewski, S. D. Poynton and R. C. T. Slade, *ECS Trans.*, 2008, 1819–1834.
123 P. V. Mazin, N. A. Kapustina and M. R. Tarasevich, *Russ. J. Electrochem.*, 2011, **47**, 275–281.
124 Q. He and X. Ren, *J. Power Sources*, 2012, **220**, 373–376.
125 X. Wang, J. P. McClure and P. S. Fedkiw, *Electrochim. Acta*, 2012, **79**, 126–132.
126 H. Wendt and G. Imarisio, *J. Appl. Electrochem.*, 1988, **18**, 1–14.
127 J. Luo, J.-H. Im, M. T. Mayer, M. Schreier, M. K. Nazeeruddin, N.-G. Park, S. D. Tilley, H. J. Fan and M. Grätzel, *Science*, 2014, **345**, 1593–1596.
128 O. Khaselev, A. Bansal and J. A. Turner, *Int. J. Hydrogen Energy*, 2001, **26**, 127–132.
129 J. Brillet, J.-H. Yum, M. Cornuz, T. Hisatomi, R. Solarska, J. Augustynski, M. Graetzel and K. Sivula, *Nat. Photonics*, 2012, **6**, 824–828.
130 R. E. Rocheleau, E. L. Miller and A. Misra, *Energy Fuels*, 1998, **12**, 3–10.
131 E. Verlage, S. Hu, R. Liu, R. J. R. Jones, K. Sun, C. Xiang, N. S. Lewis and H. A. Atwater, *Energy Environ. Sci.*, 2015, **8**, 3166–3172.
132 J. R. Varcoe, P. Atanassov, D. R. Dekel, A. M. Herring, M. A. Hickner, P. A. Kohl, A. R. Kucernak, W. E. Mustain, K. Nijmeijer and K. Scott, *Energy Environ. Sci.*, 2014, **7**, 3135–3191.
133 M. A. Hickner, A. M. Herring and E. B. Coughlin, *J. Polym. Sci., Part B: Polym. Phys.*, 2013, **51**, 1727–1735.
134 G. Couture, A. Alaaeddine, F. Boschet and B. Ameduri, *Prog. Polym. Sci.*, 2011, **36**, 1521–1557.
135 Y. Ye and Y. A. Elabd, *Macromolecules*, 2011, **44**, 8494–8503.
136 S. T. Hemp, M. Zhang, M. H. Allen, S. Cheng, R. B. Moore and T. E. Long, *Macromol. Chem. Phys.*, 2013, **214**, 2099–2107.
137 S. Liang, M. V. O'Reilly, U. H. Choi, H.-S. Shiau, J. Bartels, Q. Chen, J. Runt, K. I. Winey and R. H. Colby, *Macromolecules*, 2014, **47**, 4428–4437.
138 G. Hubner and E. Roduner, *J. Mater. Chem.*, 1999, **9**, 409–418.
139 F. Schonberger, J. Kerres, H. Dilger and E. Roduner, *Phys. Chem. Chem. Phys.*, 2009, **11**, 5782–5795.
140 M. B. McDonald, S. Ardo, N. S. Lewis and M. S. Freund, *ChemSusChem*, 2014, **7**, 3021–3027.
141 W. Gaieck and S. Ardo, *Reviews in Advanced Sciences and Engineering*, 2014, **3**, 277–287.
142 N. M. Vargas-Barbosa, G. M. Geise, M. A. Hickner and T. E. Mallouk, *ChemSusChem*, 2014, **7**, 3017–3020.

143 R. S. Reiter, W. White and S. Ardo, *J. Electrochem. Soc.*, 2016, **163**, H3132–H3134.
144 L. Ansaloni, J. R. Nykaza, Y. Ye, Y. A. Elabd and M. Giacinti Baschetti, *J. Membr. Sci.*, 2015, **487**, 199–208.
145 Y. Gu and T. P. Lodge, *Macromolecules*, 2011, **44**, 1732–1736.
146 Y. A. Elabd and M. A. Hickner, *Macromolecules*, 2010, **44**, 1–11.
147 C. M. Evans, G. E. Sanoja, B. C. Popere and R. A. Segalman, *Macromolecules*, 2016, **49**, 395–404.
148 Y. Schneider, M. A. Modestino, B. L. McCulloch, M. L. Hoarfrost, R. W. Hess and R. A. Segalman, *Macromolecules*, 2013, **46**, 1543–1548.
149 R. A. Weiss, A. Sen, L. A. Pottick and C. L. Willis, *Polymer*, 1991, **32**, 2785–2792.
150 J. Kim, B. Kim and B. Jung, *J. Membr. Sci.*, 2002, **207**, 129–137.
151 C. A. Edmondson, J. J. Fontanella, S. H. Chung, S. G. Greenbaum and G. E. Wnek, *Electrochim. Acta*, 2001, **46**, 1623–1628.
152 Y. A. Elabd, E. Napadensky, J. M. Sloan, D. M. Crawford and C. W. Walker, *J. Membr. Sci.*, 2003, **217**, 227–242.
153 Z. Shi and S. Holdcroft, *Macromolecules*, 2005, **38**, 4193–4201.
154 H. Ghassemi, J. E. McGrath and T. A. Zawodzinski Jr, *Polymer*, 2006, **47**, 4132–4139.
155 M. F. H. Schuster and W. H. Meyer, *Annu. Rev. Mater. Res.*, 2003, **33**, 233–261.
156 K. D. Kreuer, *J. Membr. Sci.*, 2001, **185**, 29–39.
157 A. Bozkurt and W. H. Meyer, *Solid State Ionics*, 2001, **138**, 259–265.
158 H. Erdemi, A. Bozkurt and W. H. Meyer, *Synth. Met.*, 2004, **143**, 133–138.
159 P. Cotanda, G. Sudre, M. A. Modestino, X. C. Chen and N. P. Balsara, *Macromolecules*, 2014, **47**, 7540–7547.
160 G. Sudre, S. Inceoglub, P. Cotanda and N. P. Balsara, *Macromolecules*, 2013, **46**, 1519–1527.
161 K. J. Noonan, K. M. Hugar, H. A. Kostalik IV, E. B. Lobkovsky, H. c. D. Abruña and G. W. Coates, *J. Am. Chem. Soc.*, 2012, **134**, 18161–18164.
162 K. Vijayakrishna, S. K. Jewrajka, A. Ruiz, R. Marcilla, J. A. Pomposo and D. Mecerreyes, *Macromolecules*, 2008, **41**, 6299–6308.
163 J. Yang, W. Sun, W. Lin and Z. Shen, *J. Polym. Sci., Part A: Polym. Chem.*, 2008, **46**, 5123–5132.
164 M. L. Hoarfrost and R. A. Segalman, *Macromolecules*, 2011, **44**, 5281–5288.
165 M. L. Hoarfrost and R. A. Segalman, *ACS Macro Lett.*, 2012, **1**, 937–943.
166 M. L. Hoarfrost, M. Tyagi, R. A. Segalman and J. A. Reimer, *J. Phys. Chem. B*, 2012, **116**, 8201–8209.
167 M. L. Hoarfrost, M. S. Tyagi, R. A. Segalman and J. A. Reimer, *Macromolecules*, 2012, **45**, 3112–3120.
168 J. M. Virgili, A. Hexemer, J. A. Pople, N. P. Balsara and R. A. Segalman, *Macromolecules*, 2009, **42**, 4604–4613.
169 N. S. Wanakule, J. M. Virgili, A. A. Teran, Z.-G. Wang and N. P. Balsara, *Macromolecules*, 2010, **43**, 8282–8289.
170 M. J. Park, K. H. Downing, A. Jackson, E. D. Gomez, A. M. Minor, D. Cookson, A. Z. Weber and N. P. Balsara, *Nano Lett.*, 2007, **7**, 3547–3552.
171 M. J. Park, A. J. Nedoma, P. L. Geissler, N. P. Balsara, A. Jackson and D. Cookson, *Macromolecules*, 2008, **41**, 2271–2277.
172 O. Kim, G. Jo, Y. J. Park, S. Kim and M. J. Park, *J. Phys. Chem. Lett.*, 2013, **4**, 2111–2117.
173 K. M. Diederichsen, R. R. Brow and M. P. Stoykovich, *ACS Nano*, 2015, **9**, 2465–2476.
174 A. Berger and J. Newman, *J. Electrochem. Soc.*, 2014, **161**, E3328–E3340.
175 Y. K. Gaudy and S. Haussener, *J. Mater. Chem. A*, 2016, **4**, 3100–3114.
176 S. Haussener, S. Hu, C. Xiang, A. Z. Weber and N. S. Lewis, *Energy Environ. Sci.*, 2013, **6**, 3605–3618.
177 S. Tembhurne, M. Dumortier, S. Haussener, Proceedings of the 15th International Heat Transfer Conference, Kyoto, Japan, 2014.
178 M. R. Singh, J. C. Stevens and A. Z. Weber, *J. Electrochem. Soc.*, 2014, **161**, E3283–E3296.
179 C. Xiang, Y. Chen and N. S. Lewis, *Energy Environ. Sci.*, 2013, **6**, 3713–3721.
180 A. C. Nielander, M. R. Shaner, K. M. Papadantonakis, S. A. Francis and N. S. Lewis, *Energy Environ. Sci.*, 2015, **8**, 16–25.
181 T. J. Jacobsson, V. Fjallstrom, M. Edoff and T. Edvinsson, *Energy Environ. Sci.*, 2014, **7**, 2056–2070.
182 S. Rau, S. Vierrath, J. Ohlmann, A. Fallisch, D. Lackner, F. Dimroth and T. Smolinka, *Energy Technol.*, 2014, **2**, 43–53.
183 T. L. Gibson and N. A. Kelly, *Int. J. Hydrogen Energy*, 2008, **33**, 5931–5940.
184 P. A. Lehman, C. E. Chamberlin, G. Pauletto and M. A. Rocheleau, *Int. J. Hydrogen Energy*, 1997, **22**, 465–470.
185 J. M. Vidueira, A. Contreras and T. N. Veziroglu, *Int. J. Hydrogen Energy*, 2003, **28**, 927–937.
186 N. A. Kelly, T. L. Gibson and D. B. Ouwerkerk, *Int. J. Hydrogen Energy*, 2008, **33**, 2747–2764.
187 A. Brinner, H. Bussmann, W. Hug and W. Seeger, *Int. J. Hydrogen Energy*, 1992, **17**, 187–197.
188 C. A. Rodriguez, M. A. Modestino, D. Psaltis and C. Moser, *Energy Environ. Sci.*, 2014, **7**, 3828–3835.
189 D. G. Nocera, *Acc. Chem. Res.*, 2012, **45**, 767–776.
190 Y. Lin, C. Battaglia, M. Boccard, M. Hettick, Z. Yu, C. Ballif, J. W. Ager and A. Javey, *Nano Lett.*, 2013, **13**, 5615–5618.
191 S. W. Boettcher, J. M. Spurgeon, M. C. Putnam, E. L. Warren, D. B. Turner-Evans, M. D. Kelzenberg, J. R. Maiolo, H. A. Atwater and N. S. Lewis, *Science*, 2010, **327**, 185–187.
192 J. R. Maiolo, B. M. Kayes, M. A. Filler, M. C. Putnam, M. D. Kelzenberg, H. A. Atwater and N. S. Lewis, *J. Am. Chem. Soc.*, 2007, **129**, 12346–12347.

193 E. Verlage, S. Hu, R. Liu, R. J. R. Jones, K. Sun, C. Xiang, N. S. Lewis and H. A. Atwater, *Energy Environ. Sci.*, 2015, **8**, 3166–3172.
194 K. Walczak, Y. Chen, C. Karp, J. W. Beeman, M. Shaner, J. Spurgeon, I. D. Sharp, X. Amashukeli, W. West, J. Jin, N. S. Lewis and C. Xiang, *ChemSusChem*, 2015, **8**, 544–551.
195 J. Newman, *J. Electrochem. Soc.*, 2013, **160**, F309–F311.
196 M. R. Shaner, K. T. Fountaine, S. Ardo, R. H. Coridan, H. A. Atwater and N. S. Lewis, *Energy Environ. Sci.*, 2014, **7**, 779–790.
197 J. M. Spurgeon, M. G. Walter, J. F. Zhou, P. A. Kohl and N. S. Lewis, *Energy Environ. Sci.*, 2011, **4**, 1772–1780.
198 M. Dumortier, S. Tembhurne and S. Haussener, *Energy Environ. Sci.*, 2015, **8**, 3614–3628.
199 M. Dumortier and S. Haussener, *Energy Environ. Sci.*, 2015, **8**, 3069–3082.
200 B. A. Pinaud, J. D. Benck, L. C. Seitz, A. J. Forman, Z. Chen, T. G. Deutsch, B. D. James, K. N. Baum, G. N. Baum, S. Ardo, H. Wang, E. Miller and T. F. Jaramillo, *Energy Environ. Sci.*, 2013, **6**, 1983–2002.